AIAA JOURNAL
Vol. 45, No. 1, January 2007

Turbulent Marginal Separation and the Turbulent Goldstein Problem

Bernhard Scheichl* and Alfred Kluwick†
Vienna University of Technology, 1040 Vienna, Austria

DOI: 10.2514/1.23518

A new rational theory of incompressible turbulent boundary-layer flows having a large velocity defect is presented on basis of the Reynolds-averaged Navier–Stokes equations in the limit of infinite Reynolds number. This wake-type formulation allows for, among others, the prediction of singular solutions of the boundary-layer equations under the action of a suitably controlled adverse pressure gradient, which are associated with the onset of marginally separated flows. Increasing the pressure gradient locally then transforms the marginal-separation singularity into a weak Goldstein-type singularity occurring in the slip velocity at the base of the outer wake layer. Interestingly, this behavior is seen to be closely related to (but differing in detail from) the counterpart of laminar marginal separation, in which the skin friction replaces the surface slip velocity. Most important, adopting the concept of locally interacting boundary layers results in a closure-free and uniformly valid asymptotic description of boundary layers that exhibit small, closed reverse-flow regimes. Numerical solutions of the underlying triple-deck problem are discussed.

Nomenclature

A = displacement function (boundary-layer theory)
$\hat{A}$ = displacement function (triple-deck theory)
$A_{+,-}$ = numerical constants in $F_+(\eta)$ and $F_-(\eta)$
B = upstream slope of U_s
$\hat{B}$ = slope of $\hat{U}_s$ near separation (triple-deck theory)
$\hat{B}_1$ = leading-order coefficient in expansion of $\hat{B}$ about $\hat{L} = \chi - \chi^* = 0$
b = constant slope $\mathrm{d}\Delta/\mathrm{d}x$ (self-preserving boundary-layer solution)
C_+ = numerical constant in $G_+(\eta)$
c_ℓ = constant in mixing length closure, $c_\ell = \alpha^{1/2}$
D = strength of perturbation of B
F = stream function (self-preserving boundary-layer solution)
$F_{+,-}$ = leading-order stream functions (locally expanded boundary-layer solutions)
$f, \bar{f}$ = stream functions (locally expanded boundary-layer solutions)
G = stream function perturbation (locally expanded boundary-layer solutions)
$g, \check{g}$ = stream function perturbations (locally expanded boundary-layer solutions)
H = auxiliary function
h = surface metric coefficient
I = intermittency factor by Klebanoff
k = surface curvature
$\hat{L}$ = bubble length
$\tilde{L}, \tilde{U}$ = reference length, reference velocity
l = local sublayer thickness
ℓ = mixing length
m = external flow exponent
m_s = external flow exponent (self-preserving boundary layer)
$\hat{P}$ = induced pressure
p = pressure
q = notation to represent a collection of quantities
$\langle q \rangle$ = Reynolds averaging of any quantity represented by q
r = exponent
Re = Reynolds number (globally defined)
$S, \hat{S}$ = local streamwise lower-deck coordinates
s = local streamwise coordinate
$\hat{s}, \hat{x}$ = shifted local streamwise coordinates
T = Reynolds shear stress (boundary-layer solution)
t, z = auxiliary variables
U, P = local representations of u_e, $\mathrm{d}p/\mathrm{d}x$
U_s = surface slip velocity (boundary-layer solution)
$\bar{U}_s$ = lower-deck representation (boundary-layer theory) of U_s
$\hat{U}_s$ = lower-deck representation (triple-deck theory) of U_s
U_+ = numerical constant in $F_+(\eta)$
u, v = velocity components in x and y direction
u_e = surface slip velocity (external potential flow)
u_s = surface slip velocity
u', v' = velocity fluctuations in x and y direction
$X, \bar{Y}$ = lower-deck coordinates (boundary-layer theory)
$\hat{X}, \hat{Y}$ = lower-deck coordinates (triple-deck theory)
$\mathcal{X}, \mathcal{Y}$ = transformed lower-deck coordinates (triple-deck theory)
x, y = natural coordinates
Y = boundary-layer coordinate
$\hat{y}$ = vertical upper-deck coordinate
$\hat{Z}$ = shifted vertical lower-deck coordinate (triple-deck theory)
α = slenderness parameter
β = control parameter
Γ = Gamma function
Γ = upstream limit of $\hat{U}_s$, similarity parameter
γ = bifurcation parameter
Δ = boundary-layer thickness (boundary-layer solution)
δ = boundary-layer thickness
ε = notion for gauge function
ϵ = bifurcation parameter (redefined)
ζ = auxiliary variable
$\eta, \hat{\eta}$ = local similarity variables based on s and $\hat{s}$
$\bar{\eta}, \check{\eta}, \breve{\eta}$ = local similarity variables
θ = Heaviside step function

Presented as Paper 4936 at the 4th AIAA Theoretical Fluid Mechanics Meeting, Toronto Ontario Canada, 6–9 June 2005; received 27 February 2006; revision received 31 July 2006; accepted for publication 31 July 2006.

*Postdoctoral Research Fellow, Institute of Fluid Mechanics and Heat Transfer, Resselgasse 3/E322; b.scheichl@tuwien.ac.at.

†Full Professor, Institute of Fluid Mechanics and Heat Transfer, Resselgasse 3/E322; a.kluwick@tuwien.ac.at. Senior member AIAA.

κ	=	von Kármán constant
Λ	=	strength of induced pressure
λ, μ	=	invariance parameters
$\tilde{\nu}$	=	kinematic viscosity
Ξ, Φ	=	coefficients in asymptotic series
ξ	=	boundary-layer coordinate Y related to Δ
ρ, ϑ	=	polar coordinates
$\hat{\rho}$, ϑ	=	polar coordinates (upper deck)
σ	=	triple-deck length scale
τ	=	surface shear stress
Υ	=	shear stress gradient evaluated at surface
ϕ	=	local scaling function
χ	=	coupling parameter
χ_b	=	upper bound of χ
Ψ	=	stream function (boundary-layer solution)
$\hat{\Psi}$, $\hat{T}$	=	lower-deck representations (triple-deck theory) of Ψ and T
$\bar{\Psi}$, $\bar{T}$	=	lower-deck representations (boundary-layer theory) of Ψ and T
ψ	=	stream function
$\hat{\psi}$, $\hat{p}$	=	upper-deck perturbations of ψ and p
Ω	=	eigenvalue
ω	=	exponent
$1a$, $1b$	=	oncoming near-surface flow regimes (boundary-layer theory)
2	=	downstream and upstream evolving main flow regimes (boundary-layer theory)
$\star$	=	dependences on unknown quantities

Subscripts

D, R	=	detachment, reattachment
G, M	=	Goldstein-type singularity, marginal-separation singularity
i	=	ith member in asymptotic series
ij	=	jth member of ith member in asymptotic series
ijk	=	kth member of jth member of ith member in asymptotic series
$+$, $-$	=	downstream and upstream (of $s = 0$ or $\hat{s} = 0$) evolving forms

Superscript

*	=	onset of separation

I. Introduction

THE method of matched asymptotic expansions has undoubtedly proven very successful not only in gaining a profound understanding of laminar high-Reynolds-number flows in many aspects, but also in providing a rational framework for a methodical and comprehensive treatment of turbulent shear layers. It is to Professor David Walker's credit (see the Acknowledgments) that he was one of the first to have elucidated the modern and fruitful asymptotic formulation of the classical two-dimensional two-tiered turbulent boundary-layer structure, which is essentially based on the assumption of an asymptotically small streamwise velocity defect with respect to the external freestream flow; see the extensive contribution [1]. For an extension to the three-dimensional case, the reader is referred to [2,3], and a summary is also given in [1]. In contrast to earlier treatments of wall-bounded turbulent shear flows put forward in the pioneering papers by, among others, Yajnik [4], Bush and Fendell [5], Fendell [6], and Mellor [7], in his thorough analysis the local (and not a characteristic) value of the skin friction velocity serves as the principal perturbation parameter. That is, leading and higher-order contributions to the well-established logarithmic law of the wall are effectively summed up to a single leading-order expression, whereas higher-order corrections are free of purely logarithmic terms. In turn, the logarithmic law of the wall appears as the limit far from the surface of the leading-order streamwise velocity distribution inside the viscous wall layer. Hence, the whole information needed for the further analysis of the outer velocity defect layer is subsumed in a single term in an elegant manner. We note that this formulation was also adopted by Gersten [8,9] and, more recently, in the further developments by the present authors [10–12]. Also, a more recent strong experimental support of that classical scaling is found in [13].

Moreover, it must be emphasized that David Walker was substantially involved in providing the initial steps toward a systematic insight into the very complex turbulent near-wall dynamics, by investigating the unsteady Navier–Stokes equations in the high-Reynolds-number limit [1,14–17].

Despite the undeniable progress, much of which must be attributed to David Walker, asymptotic methods have contributed toward an understanding of the fundamental physics of wall-bounded turbulent shear flows, a fully self-consistent theory describing turbulent boundary-layer separation in the limit of high Reynolds number is not available at the moment. In particular, the literature lacks a rational description of the, from an engineering point of view, very important case of separation from a smooth surface that is caused by a smooth adverse pressure gradient, imposed by the external flow. In laminar boundary-layer theory, this type of separation is commonly referred to as *marginal* separation, as the boundary layer may exhibit a closed reverse-flow regime at its base if the pressure gradient is properly chosen. This theory was developed independently by Ruban [18,19] and by Stewartson et al. [20]; also cf. [21]. However, a systematic approach to its turbulent counterpart has been hampered severely by the fact that, generally spoken, turbulent boundary layers are known to be less prone to separate than the corresponding laminar ones, owing to the enhanced wall shear stress. More specifically, the classical small-defect formulation is seen to withstand a smooth adverse pressure gradient, as the wall shear stress remains almost constant in the high-Reynolds-number limit. Furthermore, the velocity defect solution in the outer main layer is characterized by linearized convective terms in leading order, which indicates that it does not terminate in a singularity during downstream evolution. As a matter of fact, this property is demonstrated numerically in the preliminary work provided by [10,22] for the present investigation. Additionally, the study of turbulent separation past a blunt body by Neish and Smith [23] serves as a further strong hint that the classical description of a turbulent boundary layer exposed to a smooth adverse pressure gradient predicts firmly attached flows that do not separate at all (apart from the inevitable flow detachment close to the rear stagnation point, as is the case in the situation considered in [23]) in the limit of high Reynolds number.

The first systematic approach, however, to tackle the challenging problem of pressure-induced turbulent separation from an asymptotic viewpoint was carried out by Melnik [24,25]. He proposed a primary expansion of the flow quantities in terms of a small parameter, denoted by α, which measures the slenderness of the boundary layer and is contained in all commonly employed shear stress closures and/or fixed by experiments. For example, in the case of the algebraic mixing length model by Michel et al. [8] (see also Schlichting and Gersten [26]) it is identified with the square of the constant $c_\ell \approx 0.085$. Most important, its value appears to be essentially independent of the Reynolds number, as the latter may take on arbitrarily large values. Specifically, Melnik adopted Clauser's [27] early idea of adopting the laminarlike well-known algebraic eddy-viscosity closure for the Reynolds shear stress. We note that Clauser already concluded on semi-empirical grounds in his seminal investigation [27] that, in definite contrast to the laminar case, for turbulent boundary-layer flows, the thereby defined Reynolds number given by $1/\alpha$ remarkably takes on a fixed value. By assuming a (nondimensional) velocity defect of $\mathcal{O}(1)$ in the main body of the boundary layer, that strategy is seen to provide a powerful tool for constructing a rational novel description of turbulent boundary layers, which predicts wake-type wall-bounded flows in the limit of infinite Reynolds number and even allows for the treatment of marginal separation.

Among others, a cornerstone of Melnik's analysis is the prediction of a square-root singularity encountered by the slip velocity at the base of the outermost wake region of the boundary layer, as

separation is approached due to the occurrence of an Eulerian flow stage close to the surface. This result may be regarded as the turbulent counterpart to the celebrated Goldstein singularity [28,29] in laminar boundary-layer theory, in which the slip velocity is replaced by the wall shear stress. As a rather remarkable characteristic of the flow, however, it has recently been shown [12,22] that the pressure gradient can be controlled in a way such that the Goldstein-type singularity eventually disappears; then the slip velocity decreases regularly, vanishes in a single point but increases rapidly immediately further downstream, giving rise to an abrupt acceleration of the flow near the surface. In turn, this situation is associated with *turbulent marginal* separation.

Unfortunately, Melnik's theory [24,25] is not only incomplete, as it does not give a hint how to surmount that separation singularity within the framework of the Reynolds-averaged Navier–Stokes equations, but remains conceptually unsatisfactory, also for a number of additional reasons:

1) In definite contrast to the primary premise of α being independent of the globally defined Reynolds number as $Re \to \infty$, the approach implies that $\alpha^{1/2}\, \ell_n\, Re = \mathcal{O}(1)$ in order to account for the well-known logarithmic near-wall portion of the streamwise velocity holding upstream of separation.

2) The formation of a square-root singularity in the slip velocity, which also includes the effects due to the Reynolds shear gradient, must be taken into account, in principle. Therefore, if the Eulerian limit indeed holds (independent of a specific closure), the theory lacks an explanation why such a more general form of a singularity does not occur.

3) It remains unclear how far the asymptotic flow structure and the main results depend on Melnik's choice of the algebraic eddy-viscosity-based closure for the Reynolds shear stress in the outer wake regime.

The novel theory to be presented here is based on Melnik's formulation of turbulent boundary layers having a large velocity defect, strikingly contrasting the classical asymptotic theory. Most important, however, it also copes with the issues 1–3. In the subsequent analysis, we concentrate on the case $\alpha \ll 1$ at infinite Reynolds number, formally written as $Re^{-1} = 0$.

The paper is organized as follows: In Sec. II the essential basic assumptions underlying the theory and their implications are presented. In Sec. III we give a short survey of the numerical study of a boundary layer driven by a controlled pressure gradient toward marginal separation and the local analysis of the flow near the point of vanishing slip velocity. A particular form is assumed for the external flow velocity in terms of a single control parameter, such that the local adverse pressure gradient increases as this parameter increases. For a critical value of the parameter, a singularity appears at a certain location, indicating the first appearance of separation. As the parameter is increased slightly, the singularity is shifted a short distance upstream. The singular behavior of the flow near this point of vanishing slip velocity is summarized. Such an investigation has already been presented in [22] and will also be outlined, more extensively, in a separate investigation. The key results of the work are provided by Sec. IV, in which we focus on the local interaction of the marginally separating boundary layer with the induced external irrotational flow. The local flow is seen to have a three-layer, or *triple-deck*, structure; the appropriate limiting forms of the basic equations are presented for the different flow regions. As a highlight, akin to the laminar case [19,20], a fundamental equation governing turbulent marginal separation, which is independent of a specific shear stress closure, is derived and its solutions are discussed. Representative numerical results are shown, demonstrating the extent of the asymptotically short and flat separation bubble.

II. Motivation and Problem Formulation

A. Governing Equations

We consider a nominally steady and two-dimensional fully developed turbulent boundary layer driven by an incompressible and otherwise nonturbulent external bulk flow along a smooth and impermeable solid surface, being, for example, part of a diffuser duct

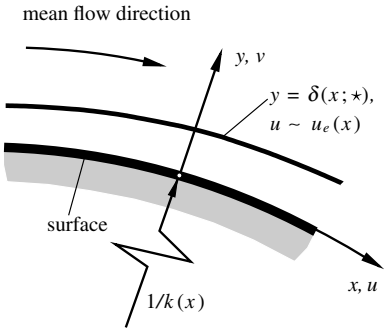

Fig. 1 Flow configuration, shown here for $k(x) > 0$.

(see Fig. 1). Let x, y, u, v, u', v', and p denote plane natural coordinates, respectively, along and perpendicular to the surface given by $y = 0$, the time-mean velocity components in the x and y directions, the corresponding turbulent velocity fluctuations, and the time-mean fluid pressure. These quantities are nondimensional, with a reference length $\tilde{L}$ characteristic for the mean velocity variation of the bulk flow along the surface (and the surface geometry), a reference value $\tilde{U}$ of the surface slip velocity due to the prescribed inviscid and irrotational external freestream flow, and the uniform fluid density. The (constant) kinematic fluid viscosity $\tilde{\nu}$ with $\tilde{L}$ and $\tilde{U}$ then define a suitable global Reynolds number, which is taken to be large:

$$Re = \tilde{U}\tilde{L}/\tilde{\nu} \to \infty \tag{1}$$

We furthermore introduce a stream function ψ by

$$\partial\psi/\partial y = u, \qquad \partial\psi/\partial x = -hv, \qquad h = 1 + k(x)y \tag{2}$$

Here, $k(x) = \mathcal{O}(1)$ is the nondimensional surface curvature, where the cases $k < 0$, $k = 0$, and $k > 0$ refer to a concave, plane, and convex surface, respectively; cf. Fig. 1. Adopting the usual notation for the turbulent stresses, the dimensionless time- or, equivalently, Reynolds-averaged Navier–Stokes equations then read (cf. [8], p. 81)

$$h\left(\frac{\partial\psi}{\partial y}\frac{\partial}{\partial x} - \frac{\partial\psi}{\partial x}\frac{\partial}{\partial y}\right)\frac{\partial\psi}{\partial y} - k\frac{\partial\psi}{\partial x}\frac{\partial\psi}{\partial y} = -h\frac{\partial p}{\partial x} - h\frac{\partial\langle u'^2\rangle}{\partial x} - \frac{\partial(h^2\langle u'v'\rangle)}{\partial y} + \mathcal{O}(Re^{-1}) \tag{3}$$

$$\left(\frac{\partial\psi}{\partial x}\frac{\partial}{\partial y} - \frac{\partial\psi}{\partial y}\frac{\partial}{\partial x}\right)\left(\frac{1}{h}\frac{\partial\psi}{\partial x}\right) - k\left(\frac{\partial\psi}{\partial y}\right)^2 = -h\frac{\partial p}{\partial y} - \frac{\partial(h\langle v'^2\rangle)}{\partial y} - \frac{\partial\langle u'v'\rangle}{\partial x} + k\langle u'^2\rangle + \mathcal{O}(Re^{-1}) \tag{4}$$

Herein, the terms of $\mathcal{O}(Re^{-1})$ refer to the divergence of the viscous stresses, which are presumed to be negligibly small compared with the Reynolds stresses throughout the boundary layer, with the exception of a viscous sublayer adjacent to the surface.

B. Novel Wake-Like Limit of Wall-Bounded Turbulent Shear Flows

A new approach to turbulent boundary layers has been developed to provide an appropriate asymptotic concept for a description of marginally separated flows. This theory is essentially founded on three key assumptions (which, although seeming plausible, nevertheless have to be validated empirically):

1) Both the velocity fluctuations u' and v' are of the same order of magnitude in the limit $Re \to \infty$, so that all Reynolds stress components are scaled equally in the whole flowfield. This requirement for local isotropy in the limit (1) is invoked quite frequently in the further analysis, but will not be addressed again then.

2) As the basic property of the flow, and already mentioned in the introduction, the streamwise velocity deficit in the main part of the

boundary layer, in which Reynolds shear predominates over molecular shear, is a quantity of $\mathcal{O}(1)$.

3) The distance $y = \delta(x; \star)$ (here, and in the following discussion, the asterisk shall indicate any further dependences) from the surface defines the time-mean outer edge of the boundary layer, as sketched in Fig. 1. This is in agreement with the observation of a rather sharp fluctuating outer edge of the time-dependent fluid motion.

1. Leading-Order Boundary-Layer Problem

As a first consequence of items 1–3 in the preceding paragraph, inspection of the equations of motion (3) and (4) suggests a shear layer approximation, for which the slenderness of the associated boundary layer is measured by a small positive parameter, denoted by $\alpha \ll 1$, such that $\delta = \mathcal{O}(\alpha)$. We, therefore, anticipate inner expansions

$$y = \alpha Y \tag{5}$$

$$\{\psi, -\langle u'v'\rangle, \delta\} = \alpha\{\Psi(x, Y), T(x, Y), \Delta(x)\} + \mathcal{O}(\alpha^2) \tag{6}$$

$$p - p_0(x) = \mathcal{O}(\alpha) \quad \text{where } \mathrm{d}p_0/\mathrm{d}x = -u_e \mathrm{d}u_e/\mathrm{d}x = \mathcal{O}(1) \tag{7}$$

Herein, $u_e(x)$ denotes the surface velocity imposed by the external potential bulk flow. Then, the main flow regime of the boundary layer is governed by the boundary-layer equations:

$$\frac{\partial\Psi}{\partial Y}\frac{\partial^2\Psi}{\partial Y\partial x} - \frac{\partial\Psi}{\partial x}\frac{\partial^2\Psi}{\partial Y^2} = u_e\frac{\mathrm{d}u_e}{\mathrm{d}x} + \frac{\partial T}{\partial Y}, \qquad T = \ell^2\frac{\partial^2\Psi}{\partial Y^2}\left|\frac{\partial^2\Psi}{\partial Y^2}\right| \tag{8}$$

where the latter relationship defines the mixing length. Equation (8) is subject to the wake-type boundary conditions:

$$\begin{aligned} &\Psi(x, 0) = T(x, 0) = 0 \\ &\frac{\partial\Psi}{\partial Y}[x, \Delta(x)] - u_e(x) = T[x, \Delta(x)] = 0 \end{aligned} \tag{9}$$

The requirements to be satisfied at the boundary-layer edge given by $y = \delta(x; \alpha, \star)$ [cf. Fig. 1] or, equivalently, $Y \sim \Delta(x)$ reflect the patch with the irrotational external flow, and the conditions holding at the base of the outer wake arise from the match with the α-dependent and Reynolds-number-dependent sublayers. These are not considered here in detail but are discussed in, respectively, [11,12] (and, in a more comprehensive manner, in a separate study) and outlined briefly in Sec. II.B.2.

Note that the solution in the outer wake region comprising most of the boundary layer is completely determined by Eqs. (8) and (9). As an important consequence arising from the boundary conditions (9), a solution of Eq. (8) gives rise to a (in general) nonvanishing slip velocity

$$U_s = \frac{\partial\Psi}{\partial Y}(X, 0) \tag{10}$$

in agreement with the boundary-layer concept already proposed by Clauser [27]. We expect nontrivial solutions of Eqs. (8) and (9), that is, wake-type solutions having $U_s \not\equiv u_e$ and $T \not\equiv 0$. In other words, inside the boundary layer the simple irrotational Eulerian, that is, nonturbulent, time-mean limit of the Navier–Stokes equations, which implies $\partial u/\partial Y \equiv 0$ and, consequently, $u = \partial\Psi/\partial Y \equiv u_e(x)$, is disregarded.

2. Does the Boundary-Layer Thickness Depend on the Reynolds Number?

Highly remarkably, dimensional reasoning and order-of-magnitude analysis suggests that the last of the boundary conditions (9) is fully equivalent to a negation of this question as far as the limit $Re \to \infty$ is concerned. As expressed by the last statement in the foregoing paragraph, the assumed streamwise velocity deficit of $\mathcal{O}(1)$ implicates that the Reynolds equations (3) and (4) admit a further limit apart from the pure Eulerian one, such that the slenderness parameter α remains indeed finite even in the formal limit $Re^{-1} = 0$.

The rationale can be subsumed as follows [8,10–12]: Dimensional and scaling arguments strongly indicate that the mixing length satisfies the well-known von Kármán near-wall law. Using the present notation, it is written as

$$\ell \sim \kappa Y/\alpha^{1/2}, \qquad Y/\alpha^{1/2} \to 0 \tag{11}$$

The relationship (11) holds in the overlap conjoining the fully turbulent part of the boundary layer and the viscous sublayer, in which the molecular shear stress has the same magnitude as its turbulent counterpart [8,10–12]. The celebrated logarithmic law of the wall is fully equivalent to the behavior of the mixing length given by Eq. (11). However, because it clearly prevents matching the flow quantities in the main part of the boundary layer and the viscous sublayer, at least one additional intermediate layer has to be introduced that provides the linear decay of the mixing length predicted by Eq. (11) at its base. Regarding the main layer, the assumed velocity defect of $\mathcal{O}(1)$, together with the resulting homogeneous boundary conditions holding for $Y \to 0$ [see Eq. (9)], then strongly suggest the absence of a viscosity-affected turbulent velocity scale in the outer main layer (as will be outlined in greater detail in a separate publication dealing with finite-Reynolds-number effects; see also [11,12]). That is, the stream function there and, as the most important consequence, the boundary-layer thickness are unaffected by the surface friction and, thus, by the strongly Reynolds-number-affected flow close to the surface, at the least to leading order. Therefore, the scaling parameter α is seen to be independent of the Reynolds number as $Re \to \infty$, and the shear stress tends to zero as $Y \to 0$.

Furthermore, we note that the mixing length ℓ is supposed to admit a finite limit in the overlap with an inner wake layer in which the scaled wall distance $Y/\alpha^{1/2}$ is of $\mathcal{O}(1)$. In turn, ℓ is a quantity of $\mathcal{O}(1)$ in both the main and the intermediate layer. There, the convective terms are linearized, because $u \sim U_s(x)$, as the turbulent velocity scale, which also measures the velocity perturbations about the slip velocity U_s, appears to be of $\mathcal{O}(\alpha^{3/4})$. We emphasize that the here-proposed behavior of ℓ is corroborated by any commonly applied mixing length closure; see the rather simple algebraic model by Michel et al. [8], for instance (see also [26]). Then, the balance between convection and the Reynolds shear stress, which is included in Eq. (8), requires that the width of the latter region is of $\mathcal{O}(\alpha^{3/2})$. As α does not depend on the Reynolds number, the Reynolds shear stress in that layer still does not match the asymptotically constant shear stress in the viscous near-wall region. Consequently, this indicates that both flow regimes are not influenced by viscous effects in leading order and are, therefore, identified as an outer and inner wake layer, respectively; see Fig. 2. It is interesting to note that the resulting asymptotic structure of the boundary layer then closely resembles that of a turbulent free shear flow, which was investigated by Schneider [30]. One major difference is the surface effect expressed by Eq. (11), giving rise to a square-root behavior of u [8,10,11] at the base of the inner wake regime, as sketched in Fig. 2, which has originally been established to hold on top of the viscous sublayer in case of a separating boundary layer; see, for example [8]. Hence, for finite values of the Reynolds number, a further layer

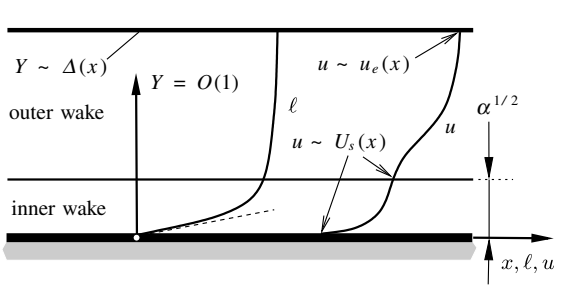

Fig. 2 Two-tiered asymptotic splitting of the boundary layer and schematic distribution of the streamwise velocity u and the mixing length ℓ in the formal limit $Re^{-1} = 0$. The dashed asymptote refers to Eq. (11).

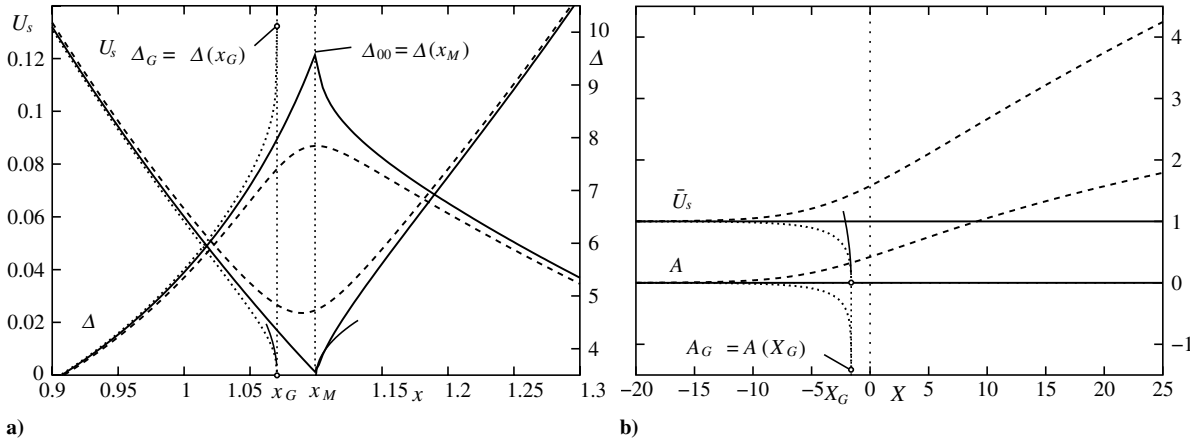

Fig. 3 Critical (solid), sub- (dashed), and supercritical (dotted) boundary-layer solutions: a) $\beta \approx \beta_M \doteq 0.84258$ (solid), $\beta = 0.8422$ (dashed), $\beta = 0.8428$ (dotted), b) canonical representation.

emerges between the viscous sublayer and the inner wake region. Therein, the Reynolds shear stress matches the wall shear stress but varies linearly with distance from the surface [10–12]. In view of the subsequent analysis, however, it is sufficient to consider the outer wake layer only. As mentioned before, here, the analysis of the remaining flow regimes is relegated to [11,12] (as well as a more detailed separate publication).

III. Singular Solutions of the Boundary-Layer Equations

Because it provides the motivation of the present analysis, it is useful to present a brief survey of [22]. In this connection we stress that we are interested primarily in particular solutions of Eqs. (8) and (9), where $U_s(x)$ vanishes locally, indicating the onset of separation.

A. Weakly Singular Numerical Solutions

To complete the turbulent boundary-layer problem, Eqs. (8) and (9) are supplemented with the simple mixing length model:

$$\ell = I(\xi)\Delta(x), \qquad I(\xi) = 1/(1 + 5.5\xi^6), \qquad \xi = Y/\Delta(x) \quad (12)$$

where the well-known intermittency factor $I(\xi)$ by Klebanoff [31] accounts for the decrease of the mixing length (and thus for an improved flow prediction) near the boundary-layer edge; cf. the experimental data presented in [32]. In fact, calculations employing the classical almost constant mixing length distribution in the outermost region [8], recovered for $I \equiv 1$, yield a slightly slower decay of the streamwise velocity near $y = \Delta(x)$ and appear to overestimate the boundary-layer thickness function $\Delta(x)$. Note that the proportionality between ℓ and the boundary-layer thickness, as predicted by the model given in Eq. (12), provides the asymptotic representation for the outer wake layer of any well-known algebraic mixing length closure. As an example, for the case $I \equiv 1$, the relationship (12) is easily obtained from the model by Michel et al. [8] (see also [26]) by formally taking the limit $c_\ell \to 0$. As already stated in Sec. I, here, α is taken to be c_ℓ^2.

Numerical solutions of the problem posed by Eqs. (8), (9), and (12) were obtained for retarded external flows that are assumed to be controlled by two parameters m_s and β, which, for example, characterize the diffuser shape, by specifying distributions of u_e of the form

$$u_e(x; m_s, \beta) = (1 + x)^{m(x;m_s,\beta)}$$

$$\frac{m}{m_s} = 1 + \frac{\beta}{1-\beta}\theta(2 - x)[1 - (1 - x)^2]^3, \qquad m_s < 0 \quad (13)$$

$$0 \le \beta < 1$$

Here, $\theta(t)$ denotes the Heaviside step function, where $\theta = 0$ for $t < 0$ and $\theta = 1$ for $t \ge 0$. It is expected, however, that other choices neither of $u_e(x)$ nor of the mixing length closure (12) will significantly affect the behavior of the solution near the location where $U_s = 0$. We also note with respect to the imposed velocity distribution (13) that in the case $\beta = 0$ (i.e., for $m \equiv m_s$), the boundary-layer equations (8) and (9) admit self-similar solutions $\Psi = \Delta F(\xi)$, $\Delta = b(1 + x)$, where $b = \text{const}$ and the position $x = -1$ defines the virtual origin of the flow, if $m_s > -1/3$. Then both the linear growth b of the boundary-layer thickness and the exponent m_s are functions of $F'(0)$, leading to a slip velocity $U_s \propto (1 + x)^m F'(0)$ [8–10,22]. These solutions were used to provide initial conditions at $x = 0$ for the downstream integration of Eqs. (8), (9), and (12), with u_e given by Eq. (13). The calculations were started by prescribing a rather small velocity defect characterized by $F'(0) = 0.95$ at $x = 0$, which, in turn, yields $b \doteq 0.3656$ and $m_s \doteq -0.3292$. Computations were then carried out for a number of positive values of β. Inspection of Eq. (13) shows that m then varies within the range $0 < x < 2$ and thus causes an additional deceleration of u_e there. The key results that are representative for the responding boundary layer are displayed in Fig. 3a.

If β is sufficiently small, the distribution of U_s is smooth, and $U_s > 0$ throughout. However, if β reaches a critical value $\beta_M \doteq 0.84258$, the surface slip velocity U_s is found to vanish at a single location $x = x_M$, but is positive elsewhere. A further increase of β provokes a breakdown of the calculations, accompanied with the formation of a weak singularity slightly upstream at $x = x_G$. An analogous behavior is observed for the boundary-layer thickness Δ, which is smooth in the subcritical case $\beta < \beta_M$, exhibits a rather sharp peak for $\beta = \beta_M$ at $x = x_M$, and approaches a finite limit Δ_G in an apparently singular manner in the supercritical case $\beta > \beta_M$.

Following the qualitatively similar behavior of the wall shear stress that replaces the slip velocity in the case of laminar boundary layers [18], here, the critical solution is termed a *marginally* separating boundary-layer solution. However, in vivid contrast to its laminar counterpart [18], it is clearly seen to be locally asymmetric with respect to the critical location $x = x_M$, where it is singular. Moreover, the turbulent solutions appear to be highly sensitive numerically to very small deviations from $\beta = \beta_M$ as $x - x_M \to 0_-$. As will turn out in the following, these closely related properties reflect the basic mechanism governing the flow in the limits $x \to x_M$ and $\beta \to \beta_M$, which is vastly different from the laminar case.

B. Marginal-Separation Singularity

To study the local flow behavior near $x = x_M$, both the outer-edge velocity u_e and the pressure gradient $\mathrm{d}p_0/\mathrm{d}x$ given by Eq. (7) are Taylor-expanded as

$$u_e = U_{00} + sU_{01} + \gamma U_{10} + \cdots$$

$$\mathrm{d}p_0/\mathrm{d}x = P_{00} + \gamma P_{10} + \cdots \quad (14)$$

$$P_{00} = -U_{00}U_{01}, \qquad P_{10} = -U_{10}U_{01}$$

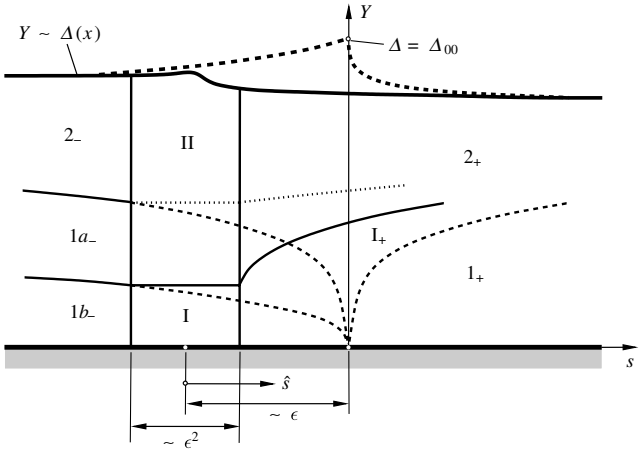

Fig. 4 Asymptotic splitting of the oncoming (subscripts −) and downstream evolving (subscripts +) boundary-layer flow in the formal limit $Re^{-1} = 0$, double-deck structure (lower deck I, main deck II). The case $\gamma \neq 0$ is sketched using solid lines, whereas the limiting structure for $\gamma = 0$ characterizing marginal separation is drawn using dashed lines partly. The flow regimes (the extent of which are marked by dotted lines) are seen to behave passively and are thus not considered in the text.

where the perturbation parameters s and γ are defined by

$$s = x - x_M \to 0, \qquad \gamma = \beta - \beta_M \to 0 \tag{15}$$

At first we focus on the critical case $\gamma = 0$. Then both the quantities Ψ and Δ are seen to assume a finite limit

$$\Psi(x, Y) \to \Psi_{00}(Y), \qquad \Delta(x) \to \Delta_{00} \quad \text{as} \quad s \to 0 \tag{16}$$

(see Figs. 3a and 4) and, in agreement with the considerations pointed out in Sec. II.B.2, inspection of Eq. (12) indicates the important relationships:

$$\ell(x, Y) \to \ell_0(Y) \quad \text{as} \quad s \to 0, \qquad \ell_0 \to \ell_{00} = \mathcal{O}(1) \quad \text{as} \quad Y \to 0 \tag{17}$$

Equation (17) provides the only empirical parameter ℓ_{00} entering the local analysis. Note that, in particular, the latter relationship in Eq. (17) is not only merely a consequence of the specific closure adopted; cf. Eq. (12). Rather, it is a consequence of the behavior of the mixing length, which, related to the two-tiered splitting of the wake regime of the boundary layer as sketched in Fig. 2, characterizes the outer wake layer.

We furthermore mention that, as a result of the limits assumed in Eqs. (16) and (17), in both the main regions 2_- and 2_+, where $Y = \mathcal{O}(1)$ (see Fig. 4), their perturbations for small values of s are governed by the convective operator in Eq. (8) only. Because of the singular behavior of the boundary-layer solution as $s \to 0$, one has to expect the occurrence of disturbances in the expansion of Ψ about its finite limit $\Psi_{00}(Y)$, which vanish as $s \to 0$ and are proportional to $\Psi'_{00}(Y)$. These perturbations represent local eigensolutions of the linear operator obtained from the corresponding linearization of Eq. (8), where $\ell = \ell_0(Y)$. However, as they do not satisfy the boundary conditions at $Y = 0$, expressed by Eq. (9), they singularly perturb that limiting value Ψ_{00}, such that for sufficiently small values of Y at least one sublayer has to be considered. There, the Reynolds stress term comes into play in leading order, as it contains the highest derivative of Ψ with respect to Y. But that means that there exists a region of a local thickness [say, $l(s)$] in which in leading order, a balance between the nonlinear convective terms and the Reynolds shear stress gradient, as provided by Eq. (8), is maintained. Then the stream function there is locally expanded as

$$\Psi = l(s)\varepsilon(s) f_0(\eta) + \cdots, \qquad \mathrm{d}\,\ell_n\,\varepsilon/\mathrm{d}s \sim l^{-3} \quad \text{as} \quad \varepsilon, l \to 0, \qquad s \to 0 \tag{18}$$

The boundary conditions (8) require $f_0(0) = f''_0(0) = 0$. A careful investigation (to be presented in a separate study) of the resulting boundary-value problem determining $f_0(\eta)$ in the case $s \to 0_-$ shows that, in order to provide a match with the expansion of Ψ about $\Psi_{00}(Y)$ in the main region 2_-, also the pressure gradient has to enter the aforementioned leading-order balance expressed by the second relationship in Eq. (18). The gauge function ε for the streamwise velocity component then is taken proportional to $(-s)^{1/2}$, giving $l \propto (-s)^{1/3}$. As a result, the momentum balance (8) is fully retained in the regions $1a_-$ and 1_+ (see Fig. 4), where the wall coordinate

$$\eta = Y/\left(\ell_{00}^{2/3}|s|^{1/3}\right) \tag{19}$$

is a quantity of $\mathcal{O}(1)$. In these flow regimes, then, the following expansions hold in, respectively, the upstream and the downstream case:

$$s \to 0_-: \ \frac{\Psi}{\ell_{00}^{2/3} P_{00}^{1/2}} = (-s)^{5/6} f_{0-}(\eta) + (-s)^{4/3} f_{1-}(\eta) + \cdots \tag{20}$$

$$s \to 0_+: \ \frac{\Psi}{\ell_{00}^{2/3} P_{00}^{1/2}} = s^{5/6} f_{0+}(\eta) + \cdots \tag{21}$$

and the resulting boundary value problem for $f_{0\mp}(\eta)$ reads

$$\begin{gathered} 1/2\, f_{0\mp}'^2 - 5/6\, f_{0\mp} f''_{0\mp} = \pm 1 \mp (f''_{0\mp})' \\ \eta = 0\text{: } f_{0\mp} = f''_{0\mp} = 0, \qquad \eta \to \infty\text{: } f_{0\mp} = O(\eta^{5/2}) \end{gathered} \tag{22}$$

where the upper and lower signs refer to the cases $s \to 0_-$ and $s \to 0_+$, respectively. The conditions at $\eta = 0$ follow from the wake-type boundary conditions (9), and the requirement for $\eta \to \infty$ reflects the match with the flow regimes 2_- and 2_+ (see Fig. 4), in which the relations (16) and (17) hold. It can be shown (as will be demonstrated in a separate paper) that in the upstream case, the problem (22) has only the obvious solution:

$$f_{0-} = F_-(\eta) = 4/15\eta^{5/2} \tag{23}$$

which expresses a balance between the Reynolds shear gradient and the adverse pressure gradient at the surface for vanishing convective terms. In turn, the match with the marginally separating profile $\Psi_{00}(Y)$ of the stream function implies

$$\Psi_{00} \sim \frac{4}{15}\frac{P_{00}^{1/2}}{\ell_{00}} Y^{5/2}, \qquad Y \to 0 \tag{24}$$

and $f_{0+} \sim F_-(\eta)$ as $\eta \to \infty$. However, in the case $s \to 0_+$, a combined analytical and numerical investigation reveals a single (strictly positive) nontrivial solution, denoted by $F_+(\eta)$, that has to be calculated numerically [22]:

$$f_{0+} = F_+(\eta), \qquad \eta \to \infty\text{: } F_+ = 4/15(\eta + A_+)^{5/2} + \mathrm{TST} \tag{25}$$

Here, and in the following discussions, TST means transcendentally small terms. It is found that

$$A_+ \doteq 1.0386, \qquad U_+ = F'_+(0) \doteq 1.1835 \tag{26}$$

As a result of the leading-order analysis, turbulent marginal separation is seen to be associated with a purely regular behavior of the flow upstream of $s = 0$, as expressed by the higher-order term in the expansion (20). Substitution into Eq. (8) yields

$$f_{1-} = B\left(\eta + \frac{\eta^4}{180}\right), \qquad B > 0 \tag{27}$$

where the constant B characterizing the slope $\mathrm{d}U_s/\mathrm{d}s \sim -BP_{00}^{1/2}$ of the linearly decreasing slip velocity in the limit $s \to 0_-$ must be determined numerically from the oncoming flow; cf. the upstream distribution of U_s in Fig. 3a. That is, the flow is locally governed by the eigensolutions $f_{0-}(\eta)$, $f_{1-}(\eta)$, and $f_{0+}(\eta)$, so that

$$s \to 0_-: \ U_s/P_{00}^{1/2} = -Bs + \cdots \tag{28}$$

$$s \to 0_+ \colon\ U_s/P_{00}^{1/2} = U_+ s^{1/2} + \cdots \tag{29}$$

Hence, the existence of the nontrivial downstream solution turns out to be responsible for the (infinitely) strong acceleration of the flow immediately downstream of the location $s = 0$ due to the irregular behavior of U_s; see Eq. (29). In turn, the convective part in Eq. (8) evaluated at $Y = 0$, given by $U_s\,\mathrm{d}U_s/\,\mathrm{d}x$, exhibits a jump at $s = 0$ from 0 to the value $P_{00}U_+^2/2$ in leading order. By adopting the numerical value $P_{00} \doteq 0.02272$, the downstream asymptote (29) is plotted as a thin solid line in Fig. 3a.

The fact that convection does not vanish necessarily at the surface $Y = 0$ not only causes the inherently nonlinear downstream behavior, governed by Eq. (22), in contrast to the theory of laminar marginal separation [18,19], but also gives rise to a fundamentally different analysis of the perturbed case $\gamma \neq 0$.

C. Bifurcating Flow for $\gamma \neq 0$

1. *Exponentially Growing Eigensolutions*

The contributions given by Eqs. (23) and (27) to the expansion (20) become of the same order of magnitude at distances s, where the new variable

$$\bar\eta = \eta/(-B^2 s)^{1/3} \tag{30}$$

is a quantity of $\mathcal{O}(1)$. This situation forces a further sublayer $1b_-$ (see Fig. 4), in which the gradients of the Reynolds shear stress and the pressure dominate over convection. Furthermore, the most rapidly downstream growing perturbations possible are assumed to originate in this layer, as their s derivatives may become asymptotically larger than the disturbances itself there, such that convection comes into play again very close to the surface. This thereby-anticipated balancing of the perturbed convective and Reynolds stress terms is required by the boundary conditions holding for $\bar\eta \to 0$. These considerations and inspection of the boundary-layer equations (8) and (9) then imply that the strongest perturbations are proportional to $\varepsilon(s)g(\bar\eta)$, where the gauge function $\varepsilon(s)$ satisfies the estimate $s^2\mathrm{d}\varepsilon/\mathrm{d}s = \mathcal{O}(\varepsilon)$ and $g(\bar\eta)$ denotes a shape function. Also, these perturbations must be due to the terms proportional to γ in Eq. (14). In turn, this suggests the following expansion in the region $1b_-$:

$$\begin{gathered}\Psi/[\ell_{00}^{2/3}P_{00}^{1/2}(-Bs)^{5/3}] = F_-(\bar\eta) + \bar\eta + \cdots + \varepsilon(s)g(\bar\eta) + \cdots \\ \varepsilon(s) = -\gamma\exp\omega(s) \\ \omega(s) = \Omega/(-B^2 s) + o(1/s), \quad \Omega > 0\end{gathered} \tag{31}$$

The higher-order contributions to the exponent $\omega(s)$ then must be determined by analyzing the higher-order terms in the expansion (31) by means of the common Fredholm alternative, in order to investigate the consecutive inhomogeneous problems (this is a topic of current research; see also [22]). The eigenvalue Ω, however, is fixed by the solution of the leading-order eigenvalue problem for the eigensolution $g(\bar\eta)$, found by linearization of Eqs. (8) and (9):

$$\begin{gathered}\Omega\,[(2/3\,\bar\eta^{3/2} + 1)g' - \bar\eta^{1/2}g] = 2(\bar\eta^{1/2}g'')' \\ g(0) = g''(0) = 0, \qquad g'(0) = D > 0\end{gathered} \tag{32}$$

Here, the unknown constant D is assumed to be fixed by the oncoming flow, such that the expansion (28) is perturbed according to

$$U_s/P_{00}^{1/2} = -Bs[1 - \gamma D\exp\omega(s)] + \cdots \tag{33}$$

A numerical study shows that problem (32) allows for a solution $g(\bar\eta)$ having subexponential growth for $\bar\eta \to \infty$ solely in the case $\Omega = 1/3$. Moreover, only in that case has the solution of problem (32) been found analytically. It reads

$$\begin{gathered}\frac{g(\bar\eta)}{D} = \frac{2}{3}\bar\eta\exp(-\bar z) + \left(\frac{2}{9}\right)^{1/3}\left(\frac{2}{3}\bar\eta^{3/2} + 1\right)\int_0^{\bar z} t^{-1/3}\exp(-t)\,\mathrm{d}t \\ \bar z = \frac{2}{9}\bar\eta^{3/2}\end{gathered} \tag{34}$$

In turn, the associated perturbation in expansion (31) provokes also exponentially small disturbances in the flow regimes $1a_-$ and $1b_-$, respectively, and in the distribution of the boundary-layer thickness $\Delta(x)$.

The question arises if there exist further perturbations if $\gamma \neq 0$ in the region $1b_-$, which locally grow faster than that considered previously and are, therefore, responsible for a breakdown of the asymptotic flow structure holding in the limit $\gamma = 0$. Consequently, we complete the analysis of the class of eigensolutions that exhibit exponential growth as $s \to 0_-$ by scrutinizing the possibility of the generation of disturbances proportional to γ that originate in a region located even closer to the surface than is the flow regime $1b_-$; see Fig. 4. This is accomplished by the introduction of the new local variables

$$\check\eta = \bar\eta/\phi(-s), \qquad \check g(\check\eta) = g(\bar\eta) \tag{35}$$

which are assumed to be quantities of $\mathcal{O}(1)$. The latter relationship in Eq. (35) expresses the match of the (for the present analysis here unknown) shape function $g(\bar\eta)$ of the respective perturbation in region $1b_-$ with that considered here, denoted by $\check g(\check\eta)$. Independent of the specific choice of the (positive) function $\phi(-s)$, substitution of the coordinate-stretching (35) into the boundary-layer equations (8) and (9) is seen to be consistent with the generalized form

$$\begin{gathered}\frac{\Psi}{\ell_{00}^{2/3}P_{00}^{1/2}(-Bs)^{5/3}\phi} = \check\eta + \phi^3 F_-(3\check\eta) + \cdots - \gamma\exp\omega(s)\check g(\check\eta) + \cdots \\ \frac{1}{\omega(s)} \to 0_+ \quad \text{as} \quad s \to 0_-\end{gathered} \tag{36}$$

of the expansion (31). In the limit

$$\phi(-s) \to 0_+ \quad \text{as} \quad s \to 0_- \tag{37}$$

under consideration, the balance between the perturbations of $\mathcal{O}(\gamma)$ of the convective terms and the Reynolds shear stress gradient requires to write

$$\omega = \omega_0(s) + o(\omega_0) \quad \text{as} \quad s \to 0_- \tag{38}$$

where ϕ can always be scaled such that

$$\omega_0'(s) = (Bs)^{-2}\phi(-s)^{-3} \quad \text{as} \quad s \to 0_- \tag{39}$$

Then the associated disturbances having a growth rate $\omega'(s)$ given by Eqs. (38) and (39), which is stronger than that implied by the expansion (31), are found to be governed by a reduced form of the problem (32). Integrated once, it reads

$$\check g = 2\check\eta^{1/2}\check g'', \qquad \check g(0) = \check g''(0) = 0, \qquad \check g'(0) > 0 \tag{40}$$

However, the solution of problem (40) exhibits exponential growth for $\check\eta \to \infty$. Consequently, no further eigensolutions with a growth rate stronger than that given by Eq. (31) are generated.

2. *Canonical Boundary-Layer Solutions*

The expansion (31) ceases to be valid within region I, the so-called lower deck (see Fig. 4), where the gauge function ε has become a quantity of $\mathcal{O}(1)$. As a consequence of its exponential growth, that region of nonuniformity takes place an asymptotically small extent upstream of $s = 0$, where $-B^2 s \sim \Omega/\ln(1/\gamma)$. With respect to the further analysis, this behavior then is conveniently expressed by introducing the coordinate shift

$$\hat s = s + \epsilon/B, \qquad \hat x = x + \epsilon/B \tag{41}$$

(see Fig. 4), and considering the limit

$$\epsilon = \Omega/(B\,\ell_n\,|D/\gamma|) \to 0, \qquad \Omega = 1/3 \tag{42}$$

Substitution of the variables

$$X = \frac{\hat{s}}{\epsilon^2}, \qquad \bar{Y} = \frac{Y}{(\ell_{00}\epsilon)^{2/3}}, \qquad \bar{\Psi}(X,\bar{Y}) = \frac{\Psi}{\ell_{00}^{2/3}P_{00}^{1/2}\epsilon^{5/3}} \tag{43}$$

which are quantities of $\mathcal{O}(1)$ in the flow regime I, into Eqs. (8) and (9) yields to leading order the reduced, that is, canonical, equations

$$\frac{\partial\bar{\Psi}}{\partial\bar{Y}}\frac{\partial^2\bar{\Psi}}{\partial\bar{Y}\partial X} - \frac{\partial\bar{\Psi}}{\partial X}\frac{\partial^2\bar{\Psi}}{\partial\bar{Y}^2} = -1 + \frac{\partial 2\bar{T}}{\partial\bar{Y}}, \qquad \bar{T} = \frac{\partial^2\bar{\Psi}}{\partial\bar{Y}^2}\left|\frac{\partial^2\bar{\Psi}}{\partial\bar{Y}^2}\right| \tag{44}$$

subject to the boundary conditions

$$\bar{Y} = 0\text{: } \bar{\Psi} = \bar{T} = 0 \tag{45}$$

$$\bar{Y} \to \infty\text{: } \partial\bar{T}/\partial\bar{Y} - 1 \to 0 \tag{46}$$

$$X \to -\infty\text{: } \bar{\Psi} \to F_-(\bar{Y}) + \bar{Y} - \mathrm{sgn}(\gamma)\exp(X/3)g(\bar{Y}) \tag{47}$$

It is furthermore useful to define the rescaled slip velocity

$$\bar{U}_s = \frac{\partial\bar{\Psi}}{\partial\bar{Y}}(X,0) \tag{48}$$

which serves to expand U_s in the form

$$U_s(X) = \epsilon P_{00}^{1/2}\bar{U}_s(x) + \cdots \tag{49}$$

and the displacement function

$$A(X) = \lim_{\bar{Y}\to\infty}(\bar{T} - \bar{Y}) \tag{50}$$

By matching with the flow in the main deck II (see Fig. 4), one obtains

$$\Psi = \Psi_{00}(Y) + \epsilon^{2/3}\ell_{00}^{2/3}A(X)\Psi'_{00}(Y) + \cdots + (\epsilon - \epsilon^2 B\hat{X})\Psi_{01}(Y) + \cdots \tag{51}$$

In turn, applying the boundary conditions given by Eq. (9), which hold for $Y = \Delta(x)$, to the expansion (51) shows that the function $A(X)$ accounts for the variation of the boundary-layer thickness in the form

$$\Delta = \Delta_{00} - \epsilon^{2/3}\ell_{00}^{2/3}A(X) + \cdots \tag{52}$$

In the critical case of vanishing γ, the resulting problem consisting of Eqs. (44–47) has the "trivial" solution $\bar{\Psi} \equiv F_-(\bar{Y})$, giving $A \equiv 0$. However, for $\gamma \neq 0$ it has to be solved numerically. The corresponding solutions are plotted in Fig. 3b. Exponential branching for $X \to -\infty$ is found as a consequence of Eq. (47), which reflects a match with the oncoming flow, as expressed by Eqs. (31) and (33), for both the quantities $\bar{U}_s(X)$ and $A(X)$. In the subcritical case $\gamma < 0$, the solution admits the nontrivial downstream state

$$X \to \infty, \qquad \bar{Y} \to \infty\text{: } \bar{\Psi}X^{-5/6} \to F_+(\eta), \qquad \eta = \bar{Y}/X^{1/3} = \mathcal{O}(1) \tag{53}$$

which implies

$$X \to \infty\text{: } A(X) \sim A_+X^{1/3}, \qquad \bar{U}_s(X) \sim U_+X^{1/2} \tag{54}$$

Equations (53) and (54) formally provide a match with the expansions (21), supplemented with Eqs. (25) and (29) if s is replaced by $\hat{s}$ there. In the latter representation, these expansions are valid in the flow regime I_+, where $0 > s = \mathcal{O}(\epsilon)$; see Fig. 4.

It is important to note that the existence of perturbations of the nontrivial solution can be demonstrated that are due to linearization and, indeed, vanish in the limit $X \to \infty$. This suggests that this specific solution effectively provides a final downstream state of the flow rather than an isolated local solution. However, as the asymptotic analysis turns out to be rather lengthy in its details, that issue will be addressed separately in a subsequent paper.

D. Goldstein-Type Singularity

For supercritical conditions $\gamma > 0$, the solution breaks down at a distinct location $X = X_G$, that is, $x = x_G$ in the original scaling; see Fig. 3. Again, this behavior is studied by means of a local similarity analysis, in which a more detailed description of the associated multilayered asymptotic structure of the local flow is presented in [22] (and will be presented in a future paper).

Introducing appropriate local variables

$$S = X - X_G, \qquad \breve{\eta} = \bar{Y}/(-S)^{1/3}, \qquad \bar{f} = \bar{\Psi}/(-S)^{5/6} \tag{55}$$

the stream function is expanded according to

$$\bar{f} = \bar{f}_0(\breve{\eta}) + (-S)^r\bar{f}_1(\breve{\eta}) + (-S)^{2r}\bar{f}_2(\breve{\eta}) + \cdots, \qquad r > 0, \quad S \to 0_- \tag{56}$$

where

$$1/2\,\bar{f}_0'^2 - 5/6\,\bar{f}_0\bar{f}_0'' = 1 - (\bar{f}_0'^2)', \qquad \breve{\eta} = 0\text{: } \bar{f}_0 = \bar{f}_0'' = 0 \tag{57}$$

cf. Eq. (22). On condition that $\bar{f}_0$ has to exhibit subexponential growth as $\breve{\eta} \to \infty$, an analytical investigation of Eq. (57) shows that this problem has two solutions, namely, $\bar{f}_0 = F_-(\breve{\eta})$ and

$$\bar{f}_0 = \sqrt{2}\,\breve{\eta} \tag{58}$$

However, only the latter solution provides a singular behavior as $S \to 0_-$. It predicts an Eulerian flow state, because the Reynolds shear stress vanishes in leading order. As a consequence,

$$\bar{U}_s \sim \sqrt{-2S}, \qquad U_s \sim \sqrt{P_{00}(x_G - x)}, \qquad x - x_G \to 0_- \tag{59}$$

The local variations of, respectively, U_s and $\bar{U}_s$ are displayed in Fig. 3 as thin solid lines.

Because Eqs. (56) and (58) cannot be matched to the profile $\bar{\Psi}(X_G,\bar{Y})$ in region II (see Fig. 4), a transitional flow regime has to be taken into account, in which the pressure gradient balances the inertia terms and $\bar{Y}/(-S)^{1/6} = \mathcal{O}(1)$. As a consequence, this further region, which is not encountered in the analysis of the marginal-separation singularity outlined in Sec. III.B, then is found to include the sublayer for which $\breve{\eta} = \mathcal{O}(1)$, considered here [22]. A further sublayer accounting for a higher-order breakdown of the expansion [Eq. (56)] emerges where $\bar{Y}/(-S)^{1/2} = \mathcal{O}(1)$. Matching with the near-wall flow there gives $r = 1/4$ and, in turn, $\bar{f}_1 \propto \breve{\eta}^{5/2}$. Likewise, the matching procedure with respect to the flow regime II in the limit $S \to 0_-$ shows that

$$A - A_G = \mathcal{O}[(-S)^{1/6}], \qquad \Delta - \Delta_G = \mathcal{O}[(x_G - x)^{1/6}] \quad \text{as} \quad x - x_G \to 0_- \tag{60}$$

as indicated by the numerical solutions presented in Fig. 3.

Solution (58) and the associated square-root behavior given by Eq. (59) has already been found by Melnik [24,25], but not in the context of marginally separated flow. It provides the analogon to the famous Goldstein singularity in laminar boundary-layer theory [18,28,29].

We note that a Goldstein-type singularity appears quite naturally by evaluating Eqs. (8) and (9) at $Y = 0$, which gives

$$U_s\mathrm{d}U_s/\mathrm{d}x \sim -P_{00} + \partial T/\partial Y, \qquad Y = 0 \quad \text{as} \quad x - x_G \to 0_- \tag{61}$$

In turn, a local square-root behavior of U_s in $x - x_G$ is suggested in general, whereas the marginal singularity characterized by the behavior (28) is seen to be a special case [25]. These results are essentially based upon the observation that Ψ and, thus, both T and

$\partial T/\partial Y$ approach finite limits as $s \to 0$ and $S \to 0_-$, respectively. However, the rather surprising fact that, in the case of the square-root singularity, $\partial T/\partial Y$ does not come into play at $S = Y = 0$ follows from the analysis of the locally self-similar behavior as expressed by Eq. (57).

IV. Local Interaction Theory for Marginally Separated Flows

In the following section, it is demonstrated how, by taking into account the locally strong interaction process between the boundary layer and the external bulk flow, the weak Goldstein-type singularity is eliminated and a uniformly valid description of the flow with respect to the Reynolds equations (3) and (4) is achieved. More precisely, it is pointed out that the locally induced pressure gradient, which is not given in advance, but rather to be determined simultaneously with the flow inside the boundary layer, must enter the analysis if $\epsilon = \mathcal{O}(\alpha^{3/10})$ or smaller. Because nonlinear convective effects cannot be neglected even near the surface, this procedure results in a triple-deck problem that, therefore, clearly differs from the formulation of laminar marginal separation [19,20], but is closely related to laminar short-scale boundary-layer interaction theory [21,33].

Note that the elliptic nature of the equations determining the induced potential flow requires the existence of a boundary-layer solution that does not terminate in a Goldstein-type singularity. Consequently, we at first assume that $\gamma \le 0$. However, the resulting interaction theory is a posteriori readily seen to apply to flows having $\gamma > 0$ also.

We furthermore stress that inspection of the equations of motion (3) and (4) indicates that the pressure gradient normal to the surface, as well as the Reynolds normal stresses, are negligibly small in any of the flow regimes considered in the subsequent investigation and will, therefore, be disregarded.

A. Induced Potential Flow

We now consider the boundary-layer solutions, assuming that $\epsilon \ll 1$, from the viewpoint of the external freestream flow, which is considered to be irrotational at least up to $\mathcal{O}(\alpha)$, because the Reynolds stresses are of $o(\alpha)$ there. That is, in the double limit $\epsilon \to 0$ and $\alpha \to 0$, the stream function and the pressure are expanded in the form

$$q = q_{00}(\hat{s}, y) + \epsilon q_{01}(\hat{s}, y) + \cdots + \alpha[q_{10}(\hat{s}, y) + \epsilon q_{11}(\hat{s}, y) + \cdots] + \mathcal{O}(\alpha^2), \quad q = \psi, p \tag{62}$$

according to the expansions (14) and (31). The coordinate shift provided by Eq. (41) ensures that the subexpansion in terms of powers of ϵ of the expansion (62) only accounts for the Taylor expansion of u_e around $\hat{s} = 0$. The terms of $\mathcal{O}(\alpha)$ reflect the streamline displacement caused by the boundary layer. Then the stream functions ψ_{00} and ψ_{10} satisfy Laplace's equation

$$\frac{\partial}{\partial \hat{s}}\left(\frac{1}{h}\frac{\partial \psi_{1i}}{\partial \hat{s}}\right) + \frac{\partial}{\partial y}\left(h\frac{\partial \psi_{1i}}{\partial y}\right) = 0, \qquad i = 0, 1 \tag{63}$$

subject to the boundary conditions

$$\psi_{00}(\hat{s}, 0) = 0, \qquad \psi_{10}(\hat{s}, 0) = \Psi_0[\hat{x}, \Delta_0(\hat{x})] - \Delta_0(\hat{x})U_0(\hat{x}) \tag{64}$$

Equation (64) follows from patching the stream function at the boundary-layer edge up to $\mathcal{O}(\alpha)$ by means of a Taylor expansion about $y = 0$, taking into account Eq. (41), and the relationship

$$u_e(x) = U_0(\hat{x}) = \frac{\partial \psi_{00}}{\partial y}(\hat{s}, 0) \tag{65}$$

Hence, ψ_{10} is seen to be determined uniquely in a certain domain $y \ge 0$ and can, in principle, be calculated by adopting standard methods. In turn, the induced pressure disturbance p_{10} follows from evaluating the linearized Bernoulli's law:

$$p_{10} = \frac{1}{h^2}\frac{\partial \psi_{00}}{\partial \hat{s}}\frac{\partial \psi_{10}}{\partial \hat{s}} - \frac{\partial \psi_{00}}{\partial y}\frac{\partial \psi_{10}}{\partial y} \tag{66}$$

We note that, without any loss of generality, in Eq. (66) any remaining pressure perturbation for vanishing velocity variations is discarded.

It is evident from inspection of Eq. (64) and the foregoing analysis of the marginally separating boundary-layer solution given by Ψ_0, Δ_0 that ψ_{10} and p_{10} behave regularly except for the location $\hat{s} = y = 0$. By defining the limiting value

$$\psi_{100} = \psi_{10}(0, 0) = \Psi_{00}(\Delta_{00}) - \Delta_{00}U_{00} \tag{67}$$

which is a quantity of $\mathcal{O}(1)$, a regular upstream but singular downstream behavior of ψ_{10} in the limit $y = 0$ and $\hat{s} \to 0$ is found. That is,

$$\hat{s} \to 0_-\colon \ \psi_{10}(\hat{s}, 0) - \psi_{100} = \mathcal{O}(\hat{s}) \tag{68}$$

$$\hat{s} \to 0_+\colon \ \frac{\psi_{10}(\hat{s}, 0) - \psi_{100}}{\ell_{00}^{2/3}U_{00}} \sim A_+\hat{s}^{1/3} \tag{69}$$

These conditions are rich enough to contain the associated singular local behavior of the pressure perturbation p_{10}. A local analysis of Eq. (63) supplemented with Eqs. (64) and (65) shows that

$$\psi_{00}/U_0(\hat{x}) = y - k(\hat{x})y^2/2 + \mathcal{O}(y^3) \quad \text{as} \quad y \to 0_+ \tag{70}$$

and

$$\frac{\psi_{10} - \psi_{100}}{\ell_{00}^{2/3}U_{00}} \sim A_+\rho^{1/3}g(\vartheta), \qquad \vartheta = \arctan(y/\hat{s})$$
$$\pi \ge \vartheta \ge 0 \quad \text{as} \quad \rho = \sqrt{\hat{s}^2 + y^2} \to 0 \tag{71}$$

where

$$g'' + g/9 = 0, \qquad g(\pi) = 0, \qquad g(0) = 1 \tag{72}$$

The solution of this problem is given by

$$g(\vartheta) = \cos(\vartheta/3) - \sin(\vartheta/3)/\sqrt{3} \tag{73}$$

Substituting Eq. (70) evaluated for $\hat{s} \to 0$, Eqs. (71) and (73) into Eq. (66) then yields

$$\frac{p_{10}}{\ell_{00}^{2/3}U_{00}^2} \sim A_+\rho^{-2/3}\left[\frac{\cos(2\vartheta/3)}{3\sqrt{3}} - \frac{\sin(2\vartheta/3)}{3}\right] \tag{74}$$

Finally, one obtains

$$\hat{s} \to 0_-\colon \ \frac{p_{10}(\hat{s}, 0)}{\ell_{00}^{2/3}U_{00}^2} \sim -\frac{2A_+}{3\sqrt{3}}\hat{s}^{-2/3} \tag{75}$$

$$\hat{s} \to 0_+\colon \ \frac{p_{10}(\hat{s}, 0)}{\ell_{00}^{2/3}U_{00}^2} \sim \frac{A_+}{3\sqrt{3}}\hat{s}^{-2/3} \tag{76}$$

Again, Eqs. (68), (69), (75), and (76) agree exactly with the behavior of the irrotational flow near the trailing edge of a flat plate that is induced by both the laminar Blasius boundary layer and the near wake. The close relationship between these two different flow configurations arising from the similarity structure of the shear layer downstream of the singular point will also be evident in the resulting interaction problem to be derived subsequently [21,34,35].

The local singularity in the induced potential flow given by Eqs. (71) and (74) indicates a breakdown of the expansions (62) for $\rho \to 0_+$, as one expects from the strong streamwise variations on a length scale of $\mathcal{O}(\epsilon^2)$ of the flow inside the boundary layer, discussed in Sec. III. As already mentioned, the higher-order contributions $q_{11}, \ldots$ to the expansions (62) do not behave more singularly. Therefore, the singularity in p_{10}, represented by Eqs. (75) and (76), and the associated response of the boundary-layer flow suffice to

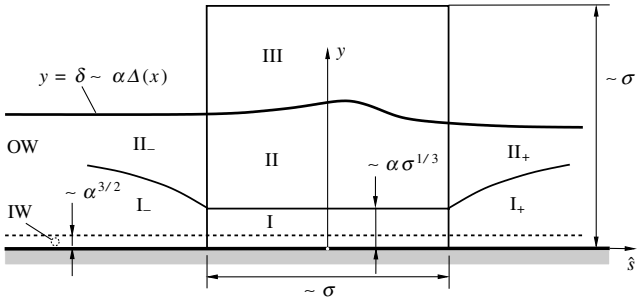

Fig. 5 Asymptotic splitting of the flow in the formal limit $Re^{-1} = 0$ due to the interaction process of the oncoming (subscripts −) and downstream evolving (subscripts +) boundary layer [outer wake (OW) and inner wake (IW); see Sec. II.B.2], triple-deck structure (lower deck I, main deck II, and upper deck III).

determine the scalings of the adjustment regions that will account for a uniformly valid flow description.

B. Triple-Deck Problem for Turbulent Boundary Layers

Because the following analysis also, necessarily, takes into account the effect of the induced pressure on the boundary layer, this section provides a revision of Sec. III.C.2. Therefore, the expansions of the quantities differ in the corresponding details. That is, here, an asymptotically correct analysis of the problem is carried out in line with the set of the full Reynolds equations (3) and (4) rather than their boundary-layer approximation given by Eqs. (8) and (9). By dealing with second-order boundary-layer theory, however, the local perturbations in the boundary layer triggered by the behavior of the induced pressure p_{10} given by Eqs. (74–76) are considered first.

In the limit $\hat{s} \to 0$, the stream function in the boundary-layer where $Y = \mathcal{O}(1)$ is given by $\psi \sim \alpha\Psi_{00}(Y)$; see Eqs. (16) and (51). We now seek the perturbations there owing to the induced pressure p_{10} upstream and downstream of $\hat{s} = 0$. Inspection of the momentum Eq. (3) in combination with the near-wall behavior given by Eq. (24) then shows that the disturbances caused by the pressure gradient $\partial p_{10}/\partial\hat{s}$ of both the Reynolds shear stress gradient and the inertia terms balance in, respectively, the regions I_- and I_+ (see Fig. 5), in which the wall coordinate

$$\hat{\eta} = Y/(\ell_{00}^{2/3}|\hat{s}|^{1/3}) \tag{77}$$

is a quantity of $\mathcal{O}(1)$. There, the following expansions are suggested in the triple limit $\epsilon \to 0$, $\alpha \to 0$, and $\hat{s} \to 0$ both for

$$\begin{aligned}\hat{s}\to 0_-\colon \frac{\psi}{\ell_{00}^{2/3}P_{00}^{1/2}} &= \alpha\Bigg[(-\hat{s})^{5/6}F_-(\hat{\eta}) + (-\hat{s})^{1/3}(\epsilon - B\hat{s})\hat{\eta} + (-\hat{s})^{4/3}\frac{B}{180}\hat{\eta}^4 \\ &\quad + \cdots\Bigg] + \alpha^2(-\hat{s})^{-5/6}\frac{\ell_{00}^{2/3}U_{00}^2}{P_{00}}G_-(\hat{\eta}) + \cdots \\ \frac{p - p_0(x_0)}{P_{00}} &= \hat{s} + \cdots - \alpha(-\hat{s})^{-2/3}\frac{2A_+}{3\sqrt{3}}\frac{\ell_{00}^{2/3}U_{00}^2}{P_{00}} + \cdots\end{aligned} \tag{78}$$

and for

$$\begin{aligned}\hat{s}\to 0_+\colon \frac{\psi}{\ell_{00}^{2/3}P_{00}^{1/2}} &= \alpha\hat{s}^{5/6}F_+(\hat{\eta}) + \cdots + \alpha^2\hat{s}^{-5/6}\frac{\ell_{00}^{2/3}U_{00}^2}{P_{00}}G_+(\hat{\eta}) + \cdots, \\ \frac{p - p_0(x_0)}{P_{00}} &= \hat{s} + \cdots + \alpha\hat{s}^{-2/3}\frac{A_+}{3\sqrt{3}}\frac{\ell_{00}^{2/3}U_{00}^2}{P_{00}} + \cdots\end{aligned} \tag{79}$$

In the expansions (78) and (79), the exponentially growing terms considered in Sec. III.C, which cause a breakdown when $\hat{s} = \mathcal{O}(\epsilon^2)$, are represented by dots. This is sufficient, as we now rather focus on the perturbations proportional to α that are responsible for the onset of the interaction process of the flow upstream and downstream of the interaction region; cf. Fig. 5.

Inserting expansions (78) and (79) into Eq. (3) and rearranging terms up to $\mathcal{O}(\alpha|2\hat{s}|^{-5/3})$ gives rise to a linear inhomogeneous third-order problem for $G_\mp(\hat{\eta})$:

$$\begin{aligned}\pm 2\left(F_\mp'' G_\mp''\right)' - \frac{5}{6}F_\mp G_\mp'' - \frac{2}{3}F_\mp' G_\mp' + \frac{5}{6}F_\mp'' G_\mp &= (-1 \mp 3)\frac{A_+}{9\sqrt{3}} \\ G_\mp(0) = G_\mp''(0) &= 0\end{aligned} \tag{80}$$

where the upper and the lower signs correspond to the upstream and the downstream case, respectively.

1. *Upstream Onset of the Interaction Process*

In the upstream case, the problem (80) assumes the form

$$\begin{aligned}(\hat{\eta}^{1/2}G_-'')' - \frac{1}{9}\hat{\eta}^{5/2}G_-'' - \frac{2}{9}\hat{\eta}^{3/2}G_-' + \frac{5}{12}\hat{\eta}^{1/2}G_- &= -\frac{2A_+}{9\sqrt{3}} \\ G_-(0) = G_-''(0) &= 0\end{aligned} \tag{81}$$

By applying the transformation

$$G_-(\hat{\eta}) = F_-'(\hat{\eta})\left[\int_0^{\hat{\eta}} \frac{H(z) - H(0)}{\zeta^{3/2}}\,\mathrm{d}\zeta - 2\frac{H(0)}{\hat{\eta}^{1/2}}\right], \qquad z = \frac{\zeta^3}{27} \tag{82}$$

Equation (81) is conveniently cast into an inhomogeneous Kummer's equation [36] for $H(z)$:

$$zH'' + (4/3 - z)H' - 7/6\,H = -A_+/9\,z^{-1/2} \tag{83}$$

where the boundary conditions in Eq. (81) require H to be bounded for $z \to 0$. In addition, the third boundary condition for G_-, missing in Eq. (81), follows from the requirement that H clearly must not grow exponentially for $z \to \infty$. The solution of Eq. (83) is found in terms of a hypergeometric series that, by using the integral representation of the Beta function [36], can be expressed in closed form as an integral. After some manipulations, we obtain

$$H(z) = \frac{A_+}{9}\frac{\pi}{2^{2/3}\Gamma(1/6)\Gamma(4/3)}\int_0^1 \frac{t^{1/6}\exp(zt)\operatorname{erfc}(\sqrt{zt})}{(1-t)^{5/6}}\,\mathrm{d}t \tag{84}$$

Inserting Eq. (84) into Eq. (82) then yields the limiting behavior of $G_-(\hat{\eta})$:

$$G_-'(0) = -A_+\frac{\sqrt{\pi}}{3\sqrt{3}} \tag{85}$$

and

$$G_- = A_- F_-'(\hat{\eta})[1 + \mathcal{O}(\hat{\eta}^{-2})] \quad \text{as} \quad \hat{\eta} \to \infty \tag{86}$$

where

$$A_- = \int_0^\infty \frac{H(z) - H(0)}{3^{3/2}z^{7/6}}\,\mathrm{d}z = -A_+\frac{2^{7/3}\Gamma(5/6)\sqrt{\pi}}{27} \tag{87}$$

We now consider the effect of the induced pressure on the surface slip velocity u_s, which is defined by

$$u_s = \partial\psi/\partial y \quad \text{at} \quad y = 0 \tag{88}$$

For distances $\hat{s} = \mathcal{O}(1)$, the surface slip is primarily given by the boundary-layer solution, that is,

$$u_s = U_s(x) + \cdots \tag{89}$$

Here, the dots denote higher-order terms due to finite values of ϵ and α. In the triple limit $\alpha \to 0$, $\epsilon \to 0$, and $\hat{s} \to 0_-$ evaluation of Eq. (78) gives

$$\frac{u_s}{P_{00}^{1/2}} = \epsilon - B\hat{s} + \cdots + \alpha(-\hat{s})^{-7/3}\frac{\ell_{00}^{2/3}U_{00}^2}{P_{00}}G'_-(0) + \cdots \tag{90}$$

where the first terms on the right-hand side represent the expansion of $U_s(x)$ about $x = x_0$, using Eq. (41). Equation (90) allows for an appealing physical interpretation: as indicated by Eqs. (78) and (85), the negative (favorable) induced pressure gradient upstream of $\hat{s} = 0$ causes a deceleration of the flow close to the surface. This rather surprising phenomenon has not been observed yet in laminar boundary-layer flows. Here, however, it originates from the fact that convection does not vanish at the surface.

Finally, matching of the expansions (78) and (79) with the flow in the boundary-layer main regimes II_- and II_+ (Fig. 5), where $Y = \mathcal{O}(1)$ demonstrates, by noticing Eq. (86), that the expansions of the stream function there take on the form

$$\hat{s} \to 0_-\colon\ \psi = \alpha[\Psi_{00}(Y) + (\epsilon - B\hat{s})\Psi_{01}(Y) + \cdots] + \alpha^2(-\hat{s})^{-4/3}\frac{\ell_{00}^{4/3}U_{00}^2}{P_{00}}A_-\Psi'_{00}(Y) + \cdots \tag{91}$$

$$\hat{s} \to 0_+\colon\ \psi = \alpha[\Psi_{00}(Y) + \hat{s}^{1/3}\ell_{00}^{2/3}A_+\Psi'_{00}(Y) + \cdots] + \alpha^2\hat{s}^{-4/3}\frac{\ell_{00}^{4/3}U_{00}^2}{P_{00}}C_+\Psi'_{00}(Y) + \cdots \tag{92}$$

It is anticipated in Eq. (92) that, in analogy to Eq. (86), the function G_+ behaves as $G_+(\hat{\eta}) \sim C_+F'_+(\hat{\eta} + A_+)$, $\hat{\eta} \to \infty$, with some constant C_+. For this mathematical detail, the reader is again referred to a future publication.

2. *Main Deck*

A breakdown of the asymptotic structure considered so far occurs due to both the exponentially growing eigensolutions when $\hat{s} = \mathcal{O}(\epsilon^2)$ [see the expansion (31) and Eq. (41)], and the singular induced pressure gradient $\partial p_{10}/\partial\hat{s}$ when $\hat{s} = \mathcal{O}(\alpha^{3/5})$; cf. the preceding expansions (91) and (92). To take into account both causes of nonuniformness, we consider a distinguished limit by introducing the coupling parameter

$$\chi = \frac{\epsilon^{10/3}}{\alpha}\frac{P_{00}}{\ell_{00}^{2/3}U_{00}^2} \tag{93}$$

which is required to be of $\mathcal{O}(1)$ in the double limit $\epsilon \to 0$ and $\alpha \to 0$. Then the streamwise distance, for which the expansions (91) and (92) cease to be valid, is found to be measured by

$$\hat{s} = \sigma\hat{X}, \qquad \sigma = (\epsilon/\Gamma)^2 \quad \text{with} \quad 0 \le \Gamma \le 1 \tag{94}$$

which, in turn, redefines the streamwise extent of the main deck (region II in Fig. 5). Here, the parameter Γ is introduced to provide a bijective function $\chi(\Gamma)$ having the properties

$$\chi'(\Gamma) > 0, \qquad \chi_b = \chi(1) \le \infty, \qquad \chi = \mathcal{O}(\Gamma^{10/3}) \quad \text{as} \quad \Gamma \to 0 \tag{95}$$

where the upper bound χ_b of the coupling parameter may be chosen arbitrarily. It is convenient with respect to the subsequent analysis to specify the relationship between Γ and χ by the definition of a further function $\Lambda(\Gamma)$ in the form

$$\chi(\Gamma) = \Gamma^{10/3}/\Lambda(\Gamma), \qquad \Lambda'(\Gamma) \le 0 \tag{96}$$

Then Λ is seen to be bounded, and

$$\Lambda(0) > \Lambda(1) = 1/\chi_b \tag{97}$$

From Eqs. (93), (94), and (96), one then readily concludes that

$$\epsilon = \sigma^{1/2}\Gamma, \qquad \alpha = \sigma^{5/3}\Lambda\frac{P_{00}}{\ell_{00}^{2/3}U_{00}^2} \tag{98}$$

The meaning of Eqs. (93–98) is as follows. The case $\chi_b = \infty$ or, equivalently, $\Lambda(1) = 0$, recovers the pure boundary-layer limit, that is, $\alpha = 0$ for finite values of ϵ, already discussed in Sec. III.C.2, for which the induced pressure gradient does not come into play at all. On the other hand, the limit $\chi = 0$ refers to the case $\gamma = \epsilon = 0$, where $\sigma = \mathcal{O}(\alpha^{3/5})$. These considerations imply that the regions I, II, and III, as sketched in Fig. 5, are located a distance of $\mathcal{O}(\epsilon)$ upstream of the position of the marginal singularity given by $s = 0$ [cf. Eq. (41)], where the lower and upper limits of the magnitude of their streamwise extent are given by $\mathcal{O}(\alpha^{3/5})$ and $\mathcal{O}(\epsilon^2)$, respectively.

Inspection of Eqs. (91) and (92) indicates that, in the main-deck region, the expansions (51) and (52) now take on the asymptotically correct forms

$$\psi/\alpha = \Psi_{00}(Y) + \sigma^{1/3}\ell_{00}^{2/3}\hat{A}(\hat{X})\Psi'_{00}(Y) + \cdots + (\sigma^{1/2}\Gamma - \sigma B\hat{X})\Psi_{01}(Y) + \cdots \tag{99}$$

and

$$\delta/\alpha = \Delta_{00} - \sigma^{1/3}\ell_{00}^{2/3}\hat{A}(\hat{X}) + \cdots \tag{100}$$

in the limit $\sigma \to 0$. Here, and in the following, the substitutions given by Eq. (98) have been applied. Moreover, the expansions (78) and (79) imply that the pressure in the main deck can be written as

$$p = p_0(x_0) + \sigma P_{00}[\hat{X} + \Lambda\hat{P}(\hat{X})] + \cdots \tag{101}$$

Both the displacement function $\hat{A}(\hat{X})$ and the pressure function $\hat{P}(\hat{X})$ are quantities of $\mathcal{O}(1)$ and are unknown at this stage of the analysis. However, matching with the regions II_- and II_+ reveals the following asymptotes:

$$\hat{X} \to -\infty\colon\ \hat{A}(\hat{X}) \sim \Lambda A_-\hat{X}^{-4/3} \tag{102}$$

$$\hat{P}(\hat{X}) \sim -\frac{2A_+}{3\sqrt{3}}\hat{X}^{-2/3} \tag{103}$$

$$\hat{X} \to +\infty\colon\ \hat{A}(\hat{X}) \sim A_+\hat{X}^{1/3} \tag{104}$$

$$\hat{P}(\hat{X}) \sim \frac{A_+}{3\sqrt{3}}\hat{X}^{-2/3} \tag{105}$$

3. *Upper Deck*

The preceding considerations suggest that the expansion (62) of the flow in the external regime, where both $\hat{s}$ and y are quantities of $\mathcal{O}(1)$, fails in the upper deck (region III in Fig. 5). There, appropriately rescaled variables are given by the scalings (94) and

$$y = \sigma\hat{y}, \qquad \hat{y} = \mathcal{O}(1) \tag{106}$$

The singular behavior of the stream function and the pressure expressed by Eqs. (69), (75), and (76) then gives rise to the expansions

$$\psi = \sigma U_{00}\hat{y} + \cdots + \Lambda\frac{P_{00}}{U_{00}}\left[\sigma^{5/3}\frac{\Psi_{100}}{\ell_{00}^{2/3}U_{00}} + \sigma^2\hat{\psi}(\hat{X},\hat{y}) + \cdots\right] \tag{107}$$

$$p = p_0(x_0) + \sigma P_{00}[\hat{X} + \Lambda\hat{p}(\hat{X},\hat{y})] + \cdots \tag{108}$$

Here, terms proportional to Λ represent the potential flow induced locally by the boundary-layer displacement.

The pressure $\hat{p}$ is calculated from Bernoulli's law [cf. Eq. (66)], which, by balancing terms up to $\mathcal{O}(\sigma^2)$, reduces to

$$\hat{p} = -\frac{\partial \hat{\psi}}{\partial \hat{y}} \tag{109}$$

and the stream function $\hat{\psi}$ is seen to satisfy the Cauchy problem:

$$\begin{gathered} \frac{\partial^2 \hat{\psi}}{\partial \hat{X}^2} + \frac{\partial^2 \hat{\psi}}{\partial \hat{y}^2} = 0, \qquad \hat{\psi}(\hat{X}, 0) = \hat{A}(\hat{X}) \\ \hat{\psi} \sim A_+ \hat{\rho}^{1/3} g(\vartheta) \quad \text{as} \quad \hat{\rho} = \sqrt{\hat{X}^2 + \hat{y}^2} \to \infty \end{gathered} \tag{110}$$

Herein, ϑ is given by Eq. (71), where the ratio $y/\hat{s}$ is to be replaced by $\hat{y}/\hat{X}$ according to the local scaling provided by Eqs. (94) and (106). The boundary conditions in Eq. (110) follow from patching the stream function at the boundary-layer edge by using Eqs. (99) and (100) and from a match of $\hat{\psi}$ with the singular behavior of ψ_{10} given by Eq. (71), respectively. In turn, $\hat{p}$ matches the asymptotic behavior of p_{10} as expressed by Eqs. (74–76). Additionally, comparing Eq. (108) with Eq. (101) and taking into account Eq. (109) yields the relationship

$$\frac{\partial \hat{\psi}}{\partial \hat{y}}(\hat{X}, 0) = -\hat{P}(\hat{X}) \tag{111}$$

where $\hat{P}(\hat{X})$ is seen to be the induced surface pressure. Consequently, and as a well-known result from potential flow theory [33], $\hat{P}(\hat{X})$ and $-\hat{A}'(3\hat{X})$ form a Hilbert pair, that is,

$$\{\hat{P}(\hat{X}), -\hat{A}'(\hat{X})\} = \frac{1}{\pi} \oint_{-\infty}^{\infty} \frac{\{\hat{A}'(\hat{S}), \hat{P}(\hat{S})\}}{\hat{X} - \hat{S}} \mathrm{d}\hat{S} \tag{112}$$

4. Lower Deck

The analysis is finalized by considering the flow in the lower deck (region I in Fig. 5) in the limit $\sigma \to 0$. Hence, we introduce rescaled local variables $\hat{Y}$ and $\hat{\Psi}$ of $\mathcal{O}(1)$ according to

$$\frac{Y}{\ell_{00}^{2/3}} = \sigma^{1/3} \hat{Y}, \qquad \frac{\psi}{\ell_{00}^{2/3} P_{00}^{1/2}} \sim \alpha \sigma^{5/6} \hat{\Psi}(\hat{X}, \hat{Y}) \tag{113}$$

Moreover, the pressure is given by Eq. (101). The leading-order problem governing the flow in the lower deck is found by inserting these quantities into the equations of motion (3) and (4) or, equivalently, by applying the transformation

$$\hat{X} = \Gamma^2 X, \qquad \hat{Y} = \Gamma^{2/3} \bar{Y}, \qquad \hat{\Psi} = \Gamma^{5/3} \bar{\Psi} \tag{114}$$

to Eq. (43). As a result, the inclusion of the induced pressure gradient in Eq. (44) is seen to be sufficient to generate an asymptotically correct description of the flow near the surface. The lower-deck equations then read

$$\begin{gathered} \frac{\partial \hat{\Psi}}{\partial \hat{Y}} \frac{\partial^2 \hat{\Psi}}{\partial \hat{Y} \partial \hat{X}} - \frac{\partial \hat{\Psi}}{\partial \hat{X}} \frac{\partial^2 \hat{\Psi}}{\partial \hat{Y}^2} = -1 - \Lambda(\Gamma) \hat{P}'(\hat{X}) + \frac{\partial \hat{T}}{\partial \hat{Y}} \\ \hat{T} = \frac{\partial^2 \hat{\Psi}}{\partial \hat{Y}^2} \left| \frac{\partial^2 \hat{\Psi}}{\partial \hat{Y}^2} \right| \end{gathered} \tag{115}$$

They are subject to the boundary conditions

$$\hat{Y} = 0\text{: } \hat{\Psi} = \hat{T} = 0 \tag{116}$$

$$\hat{Y} \to \infty\text{: } \hat{T} - \hat{Y} \to \hat{A}(\hat{X}) \tag{117}$$

$$\hat{X} \to -\infty\text{: } \hat{\Psi} \to F_-(\hat{Y}) + \Gamma \hat{Y}, \qquad 0 \le \Gamma \le 1 \tag{118}$$

$$\hat{X} \to \infty, \hat{Y} \to \infty\text{: } \hat{\Psi} \hat{X}^{-5/6} \to F_+(\hat{\eta}), \qquad \hat{\eta} = \hat{Y}/\hat{X}^{1/3} = \mathcal{O}(1) \tag{119}$$

The conditions (117–119) follow from a match with the expansions (78), (79), and (99), respectively, which clearly cease to be valid in the lower-deck flow regime. The asymptotic behavior expressed by relationship (117), however, can be shown to be determined by the upstream initial condition (118) rather than provide an additional boundary condition to be imposed. Most important, because both the functions $\hat{P}(\hat{X})$ and $\hat{A}(\hat{X})$ are seen to be part of the solution, Eqs. (115–119) have to be supplemented with one of the relationships given by Eq. (112) in order to complete the triple-deck problem.

This fundamental problem that governs turbulent marginal separation associated with the triple-deck scheme outlined previously has the following important properties:

1) As a highly remarkable characteristic not known in laminar triple-deck theory at present (apart from a laminar supersonic triple-deck flow model proposed by Lipatov [37]), the lower-deck equations (115) include both the (locally constant) imposed and the induced streamwise pressure gradient given by $\Lambda \hat{P}'(\hat{X})$.

2) A property also not observed in subsonic laminar interacting boundary layers so far is that turbulent marginal separation is linked to the existence of eigensolutions of the underlying triple-deck problem. In this connection we note that Eqs. (112) and (115–119) allow for the trivial solution $\hat{\Psi} = F_-(\hat{Y}) + \Gamma \hat{Y}$, $\hat{A}(\hat{X}) = \hat{P}(\hat{X}) = 0$. However, a nontrivial solution is conveniently enforced by prescribing the downstream condition (119). Therefore, the ellipticity of the triple-deck problem is not only due to the imposed pressure gradient [cf. Eq. (112)], but also arises from the nontrivial downstream state as expressed by Eq. (119) and in agreement with Eq. (53).

3) It is inferred from Eq. (96) that the triple-deck solutions depend on χ solely, independent of the specific choice of the function $\Lambda(\Gamma)$. This is also expressed by the invariance properties

$$\begin{gathered} \hat{\Psi}(\hat{X}, \hat{Y}) = \lambda^{-5/6} \hat{\Psi}(\mathcal{X}, \mathcal{Y}), \qquad \hat{A}(\hat{X}) = \lambda^{-1/3} \hat{A}(\mathcal{X}) \\ \hat{P}(\hat{X}) = \lambda^{2/3} \hat{P}(\mathcal{X}), \qquad \mathcal{X} = \lambda(\hat{X} - \mu), \qquad \mathcal{Y} = \lambda^{1/3} \hat{Y} \end{gathered} \tag{120}$$

satisfied by the solution $\hat{\Psi}$, $\hat{A}$, $\hat{P}$ for a given value of χ. Here, $\hat{X}$ is stretched by an arbitrary factor $\lambda > 0$. The real parameter μ corresponds to an origin shift in $\hat{X}$ of the solution. However, the ambiguity of the solution expressed by that translation invariance has to be eliminated by the exponentially decreasing eigensolutions occurring upstream, giving

$$\begin{aligned} \hat{\Psi} = {} & F_-(\hat{Y}) + \Gamma \hat{Y} + \cdots - \operatorname{sgn}(\gamma) \Gamma^{5/3} f(\hat{Y}/\Gamma^{2/3}) \\ & \times \exp[\hat{X}/(3\Gamma^2)] + \cdots, \qquad \hat{X} \to -\infty \end{aligned} \tag{121}$$

This expansion follows directly from Eq. (47) by taking into account Eq. (114). Equation (121) states that, in definite contrast to the noninteractive case that is expressed by $\Gamma = 1$ and $\Lambda = 0$ or, equivalently, Eq. (44), the interaction process is insensitive to the sign of γ. The latter rather enters the triple-deck solution only via exponentially small terms. Their strength is fixed by the requirement of a match with the oncoming flow, which, in turn, eliminates the translation invariance of the solution by means of an adequate choice of the group parameter μ.

It is useful to introduce the rescaled surface slip velocity

$$\hat{U}_s = \frac{\partial \hat{\Psi}}{\partial \hat{Y}}(\hat{X}, 0) \tag{122}$$

A comparison with Eq. (90) gives

$$u_s \sim \sigma^{1/2} P_{00}^{1/2} \hat{U}_s \quad \text{as} \quad \hat{X} = \mathcal{O}(1) \tag{123}$$

and by matching of Eq. (122) with Eq. (78) or, equivalently, Eq. (90), and Eq. (79), one recovers the expansions holding upstream and downstream, respectively,

$$\hat{X} \to -\infty\colon\ \hat{U}_s \sim \Gamma - \Lambda G'_-(0)\hat{X}^{-7/6} \tag{124}$$

$$\hat{X} \to +\infty\colon\ \hat{U}_s \sim U_+\hat{X}^{1/2} \tag{125}$$

The latter of these relationships reflects the match with the nontrivial self-similar solution expressed by $F_+(\hat{\eta})$. The asymptotic behavior [Eq. (124)] is seen to be valid for all admissible values of Γ and Λ and demonstrates the effects of both the exponentially decaying eigensolutions and of the induced pressure gradient on the triple-deck solution. The first determines the magnitude of the control parameter ϵ and, in turn, Γ, which fixes the upstream limit of the surface slip. The upstream deceleration of the flow, however, is primarily caused by the induced pressure gradient, the strength of which is measured by Λ.

As a consequence of Eqs. (115) and (116), and by noting the definition of $\hat{U}_s$ [Eq. (122)], one obtains the near-wall asymptotes:

$$\begin{aligned} \hat{\Psi} &= \hat{U}_s(\hat{X})\hat{Y} + 4/15\,\mathrm{sgn}(\Upsilon)|\Upsilon|^{1/2}\hat{Y}^{5/2} + \mathcal{O}(\hat{Y}^4) \\ \hat{T} &= \Upsilon\hat{Y} + \mathcal{O}(\Upsilon\hat{Y}^{5/2}, \hat{Y}^4) \\ \Upsilon(\hat{X}) &= \hat{U}_s(\hat{X})\hat{U}'_s(\hat{X}) + 1 + \Lambda\hat{P}'(\hat{X}), \qquad \hat{Y} \to 0 \end{aligned} \tag{126}$$

Furthermore, as already indicated by the asymptotic behavior [Eq. (25)] of the downstream similarity solution, for large values of $\hat{Y}$, the solution is seen to be invariant with respect to a shift in $\hat{Y}$ of the amount $\hat{A}(\hat{X})$. In other words, a nonvanishing value of A_+ enforces the nontrivial eigensolution of the triple-deck problem having $\hat{A} \not\equiv 0$. On the other hand, one draws the conclusion that the possible shift is an immediate consequence of the hyperbolic convective operator giving rise to the predominating convective terms, far from the surface, on the left-hand side of the momentum balance in Eq. (115). By taking into account the upstream asymptotes given by Eq. (118) together with $\hat{P}(-\infty) = 0$, the analysis then yields

$$\begin{aligned} \hat{\Psi} &= F_-(\hat{Z}) + 3/4\,\Lambda\hat{P}\hat{Z}^{-1/2} - 9/56\,\Gamma\Lambda\hat{P}\hat{Z}^{-2} \\ &\quad + \hat{Z}^{-7/2}\sum_{n=0}^{\infty}\Phi_n\hat{Z}^{-3n/2} + \mathrm{TST} \\ \hat{T} &= \hat{Z} + 9/8\,\Lambda\hat{P}\hat{Z}^{-2} - 27/14\,\Gamma\Lambda\hat{P}\hat{Z}^{-7/2} \\ &\quad + \hat{Z}^{-5}\sum_{n=0}^{\infty}\Xi_n\hat{Z}^{-3n/2} + \mathrm{TST}, \qquad \hat{Z} = \hat{Y} + \hat{A} \to \infty \end{aligned} \tag{127}$$

We note that the algebraic terms following the leading-order contributions in these asymptotic expansions vanish if, and only if, $\Lambda = 0$. To be more precise, both the leading-order coefficients Φ_0 and Ξ_0 in the remainder series are quantities of $\mathcal{O}(\Lambda, \Lambda^2, \Lambda\Gamma^2)$. One also easily verifies the match of Eq. (127) with the higher-order contribution determined by $G_-(\hat{\eta})$ to the expansion (78), which characterizes the oncoming flow, in the limit $\hat{\eta} \to \infty$; see Eqs. (86), (87), and (102).

C. Numerical Results

1. Method

For the numerical treatment of the triple-deck problem posed by Eqs. (112) and (115–119), a carefully devised variable transform that maps the interval $-\infty < \hat{X} < \infty$ onto the range $[-1, 1]$ was performed to handle the singular upstream and downstream behavior at infinity in an efficient manner. In addition, a coordinate stretching in $\hat{Y}$ direction was introduced that, among others, accounts for the far-field relationships given by Eq. (127), in which only the terms larger than the remainder sums were regarded. Most important, however, it regularizes the half-power behavior $\hat{\Psi} = \hat{U}_s(\hat{X})\hat{Y} + \mathcal{O}(\hat{Y}^{5/2})$ for $\hat{Y} \to 0$ [see Eq. (126)] and thus allows for a higher resolution of the flow close to the surface. These ideas were put forward in its original form by Smith and Merkin [38]; see also [39,40]. The thereby-transformed equations were discretized on a uniformly spaced mesh by approximating all derivatives using central finite differences with second-order accuracy. Therefore, the elliptic character of the problem is fully retained. The stream function and the pressure served as the only dependent variables. The resulting system of nonlinear algebraic equations was solved directly by adopting a modification of the Powell hybrid method [41] in which the Jacobians are calculated numerically in principle but, whenever feasible, updated by means of a secant approximation during the Newton iteration. In each Newton step, the resulting linear system of equations are solved by advantageously exploiting the sparsity pattern of the Jacobian. Under reasonable conditions, this algorithm guarantees a fast rate of global convergence. We note that, typically, a grid of 300 points in $\hat{X}$ direction and 150 points in $\hat{Y}$ direction was employed, for which the principal limit of resolution depends on the hardware memory available. The stopping criterion for the iteration process was provided by the machine-dependent optimal accuracy of the solution. It should be stressed that the indeterminacy of the solutions with respect to a shift of the origin, expressed by Eq. (120) and discussed in the preceding item 3, is eliminated numerically as a consequence of the discretization process. A more detailed description of the numerical procedure, however, is postponed to a separate publication. In addition, the authors annotate that, if applied to a broader class of problems arising in the field of interacting boundary layers, the technique presented here is even supposed to prove superior to miscellaneous well-established numerical schemes that are purpose-built for tackling such problems. Nevertheless, this is a topic that is yet under investigation.

2. Exemplary Flow Configurations

Numerical solutions have been obtained for several values of Λ, whereas Γ varied in the whole range $0 \le \Gamma \le 1$. Owing to the limitation of space, only the case $\Lambda = 3$ will be discussed in detail. It then follows from Eq. (96) that $\chi = \Gamma^{10/3}/3$ and $0 \le \chi \le \chi_b$ with $\chi_b = 1/3$. Separation is associated with negative values of $\hat{U}_s$. As an important result, such local flow reversal is observed for $0 \le \Gamma \le \Gamma^*$, where $\Gamma^* \doteq 0.205$, that means within the (rather small) range $0 \le \chi \le \chi^*$ with $\chi^* \doteq 1.69 \times 10^{-3}$. We furthermore emphasize that the shear stress gradient at the surface, given by $\Upsilon = (\partial\hat{T}/\partial\hat{Y})(\hat{X}, 0)$ as expressed in Eq. (126), and, in turn, both the Reynolds stress $\hat{T}$ and the streamwise velocity gradient $\partial^2\hat{\Psi}/\partial\hat{Y}^2$ are seen to be positive for all admissible values of $\hat{X}$, $\hat{Y}$, and χ.

Representative numerical results are plotted in Fig. 6, in which consecutive data points are connected using smooth cubic spline interpolation. In Figs. 6a and 6b the positions at the surface $\hat{Y} = 0$ of flow detachment $\hat{X} = \hat{X}_D$ (dashed curves), flow reattachment $\hat{X} = \hat{X}_R$ (dotted curves), and their difference, that is, the length

$$\hat{L} = \hat{X}_R - \hat{X}_D \tag{128}$$

of the recirculation region (solid curves) are presented in the range $0 \le \Gamma \le 0.016$ and $0.017 \le \Gamma \le 0.205 \doteq \Gamma^*$, respectively. Note that the location of detachment tends to $-\infty$ for $\Gamma \to 0$; cf. Eq. (124). In turn, a rather flat separation bubble emerges for values of Γ within the range $0 < \Gamma < 0.017$. For larger values of Γ, that is, for $\Gamma \ge 0.016\ldots$, up to $\Gamma = 0.019\ldots$ the interesting phenomenon of intermediate reattachment followed by a second flow detachment immediately further downstream is noticed. The corresponding values of $\hat{X}_D$, $\hat{X}_R$, and $\hat{L}$ characterizing that first separated flow regime (which, however, appears to be very small and, therefore, difficult to resolve numerically) are shown in Fig. 6c. Exemplarily, in Fig. 6d, the distributions of $\hat{A}(\hat{X})$, $\hat{P}(\hat{X})$, and $\hat{U}_s(\hat{X})$ are displayed for the case $\Gamma = 0.019$, together with the upstream and downstream asymptotes (dashed-dotted lines) given by Eqs. (103–105) and (125). Note the rather flat passage of the quantities $\hat{A}$ and $\hat{U}_s$ to negative values compared with their pronounced rise downstream of reattachment. As a matter of fact, the indicated splitting of the separation bubble is hardly visible and, therefore, rather a conjecture at the present stage of the numerical analysis. Thus, its validation is

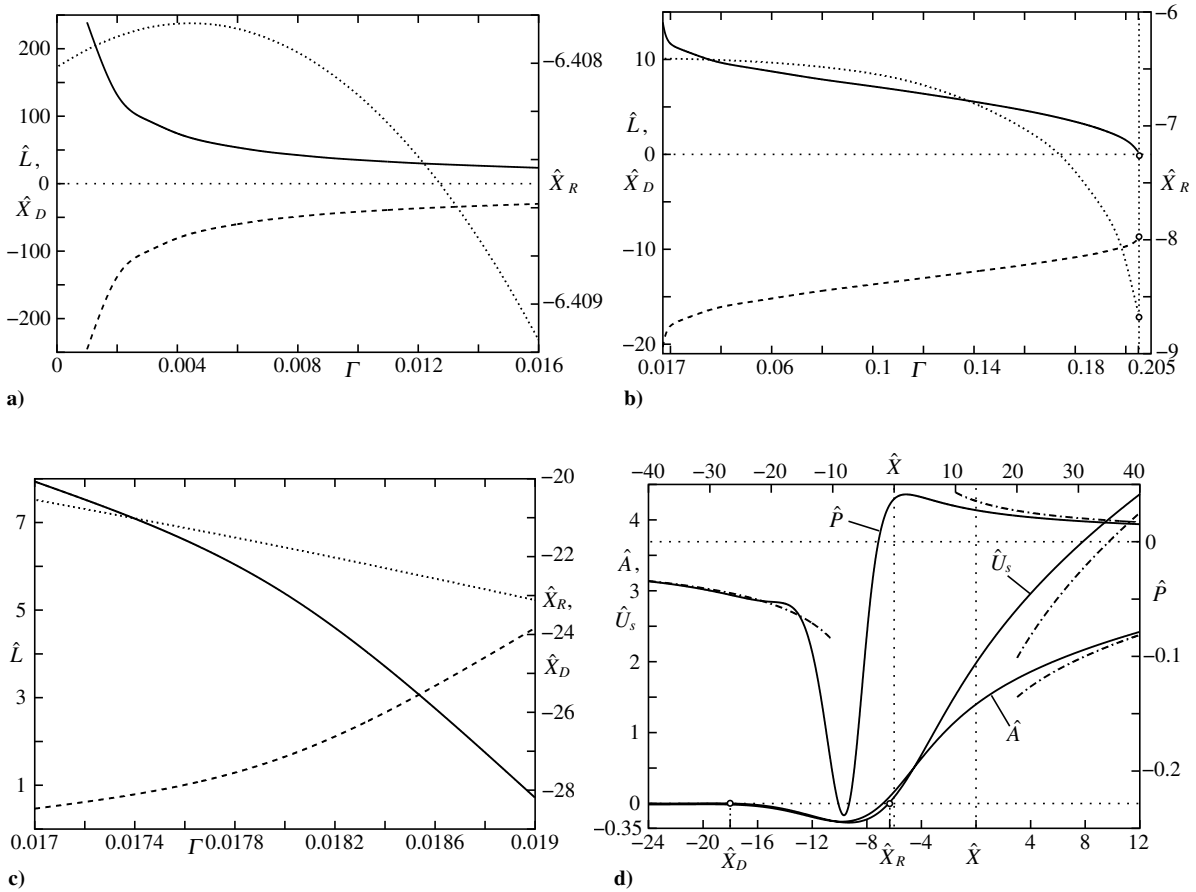

Fig. 6 Numerical solutions of the fundamental interaction problem [Eqs. (112) and (115–119)]: a)–c) locations of detachment $\hat{X} = \hat{X}_D$, reattachment $\hat{X} = \hat{X}_R$, and bubble length $\hat{L} = \hat{X}_R - \hat{X}_D$ in dependence of Γ, where c) applies to the first-separating flow regime, and d) solutions for $\Gamma = 0.019$. Here, $\hat{X}_D \doteq -18.01$ and $\hat{X}_R \doteq -6.40$. The abscissa at the bottom refers to $\hat{A}$ and $\hat{U}_s$; the one at the top refers to $\hat{P}$.

effectively a topic of further numerical effort as it requires the use of an adequately refined mesh.

In addition, both the streamline pattern and the corresponding distributions of $\hat{\Psi}$ for various $\hat{X}$ locations for the reverse-flow regime of the identical flow configuration are depicted in Fig. 7. Note the increasing density of the streamlines further away from the surface and downstream of reattachment, the latter reflecting the strong acceleration there as represented by the correspondingly rapid rise of $\hat{U}_s$. The behavior of the streamlines in the vicinity of $\hat{X} = \hat{X}_D$ and $\hat{X}_R$, respectively, is discussed in Sec. IV.C.3, next. The graphs shown in Fig. 7b agree well with the local analytical representation of $\hat{\Psi}$ given in Eq. (126).

It is noteworthy that the rather rapid acceleration of the near-wall portion of the streamwise velocity immediately downstream of reattachment indicates an intense vortex motion there. This observation is in remarkable agreement with the findings of Perry and Fairlie [42], based on their heuristic inviscid flow model. However, here, the steep rise of $\hat{U}_s$ owes to the specific internal structure of the flow ensuing from a nontrivial eigensolution of the triple-deck problem defined by Eqs. (112) and (115–119). This, in turn, owes to the strongly Reynolds-stress-affected downstream state of the solution enforced by the latter relationship.

3. *Analysis of Small Backflow Regions*

Let $\hat{X} = \hat{X}_0$ denote the point of flow detachment or reattachment. Then the slip velocity and the induced pressure gradient behave as

$$\hat{U}_s = \hat{B}(\chi)\hat{S} + \mathcal{O}(\hat{S}^2), \qquad \hat{P}' = \hat{P}_0(\chi) + \mathcal{O}(\hat{S}) \qquad \hat{S} = \hat{X} - \hat{X}_0 \to 0 \tag{129}$$

where $\hat{B} < 0$, $\hat{S} < 0$ and $\hat{B} > 0$, $\hat{S} > 0$ in, respectively, the detaching and the reattaching case. Therefore, it is readily found from substituting the expression for $\hat{U}_s$ in Eq. (129) into the first of the relationships (126), that the branching streamline having $\hat{\Psi} = 0$ is locally given by

$$\hat{Y}|_{\hat{\Psi}=0} \sim \frac{(15\hat{B})^{2/3}}{[16(1 + \Lambda\hat{P}_0)]^{1/3}}\,\hat{S}^{2/3} \tag{130}$$

cf. Fig. 7a. The term in parentheses in the denominator of Eq. (130) represents the Reynolds stress gradient at the surface given by Υ, which is seen to be positive for all values of $\hat{X}$ [cf. Eqs. (115) and (126)], here evaluated for vanishing convection (that is, for $\hat{X} = \hat{X}_0$, it reduces to the overall pressure gradient $1 + \Lambda\hat{P}'$). In connection with the infinite streamline curvature at $\hat{S} = 0$ predicted by Eq. (130) it is interesting to note that there is experimental evidence [43] that the streamline angle to the surface is not small even in the case of mild flow separation, despite the fact that the wall is flat. In this context, the authors also refer to the statements given in [23] in respect of turbulent massive separation.

The points $\hat{X} = \hat{X}_D$ and $\hat{X} = \hat{X}_R$ denoting separation and reattachment, respectively, collapse onto the single point $\hat{X} = \hat{X}^*$ for $\chi = \chi^*$, so that $\hat{B}(\chi^*) = \hat{L} = 0$. Consequently, the emergence of a small, closed reverse-flow regime is described by the relationships

$$\hat{U}_s = \hat{B}_1(\hat{S}^2 - \hat{L}^2/4) + \mathcal{O}(\hat{L}^3), \qquad \hat{P}' = \hat{P}_0(\chi^*) + \mathcal{O}(\hat{L})$$
$$\hat{X}_D = \hat{X}^* - \hat{L}/2, \qquad \hat{X}_R = \hat{X}^* + \hat{L}/2$$
$$\hat{S} = \hat{X} - \hat{X}^* = \mathcal{O}(\hat{L}), \qquad \hat{L} \to 0_+ \tag{131}$$

where a match with the expression for U_s in Eq. (129) requires

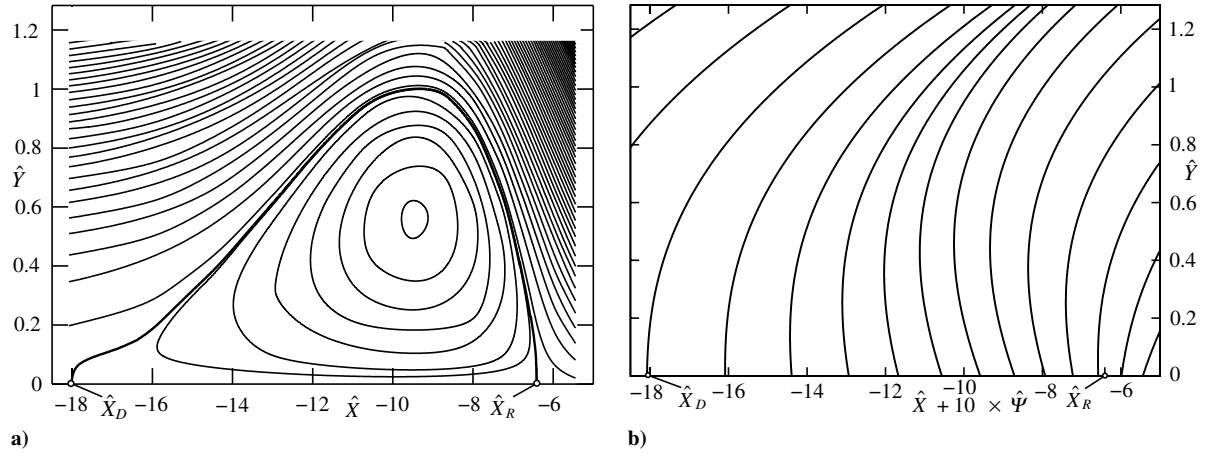

Fig. 7 Separation for the case $\Gamma = 0.019$: a) streamlines $\hat{\Psi} = \text{const}$ in the range $-0.085 \le \hat{\Psi} \le 1.01$, for which Bezier spline interpolation was applied such that the values of $\hat{\Psi}$ for neighboring curves differ by 0.015; in addition, the dividing streamline (bold) is approximated by $\hat{\Psi} = 10^{-10}$ and is rather adjacent to the one for which $\hat{\Psi} = -0.001$, which is also plotted, and b) several profiles of the stream function $\hat{\Psi}$ for the same $\hat{X}$ and $\hat{Y}$ range as in Fig. 7a, magnified by a factor of 10.

$$\hat{B} = \mp \hat{B}_1 \hat{L} + \mathcal{O}(\hat{L}^2), \qquad \hat{B}_1 > 0 \tag{132}$$

Here, the upper and the lower signs refer to, respectively, the position of separation and reattachment in Eq. (129). As the slip velocity $\hat{U}_s$ varies with χ in a regular manner, the relations (131) state that $\hat{L}$ depends on $\chi^* - \chi$ in the form

$$\hat{L} = \mathcal{O}(\sqrt{\chi^* - \chi}), \qquad \chi^* - \chi \to 0_+ \tag{133}$$

This property is captured by the behavior of the numerical results near the endpoints of the curves, indicated by circles, for which $\Gamma = \Gamma^*$ in Fig. 6b. In addition, one readily finds that the streamlines $\hat{\Psi} = \text{const}$ in the vicinity of a very mild separation bubble of length $\hat{L} \ll 1$ are given by

$$\hat{B}_1 \left(\hat{S}^2 - \frac{\hat{L}^2}{4} \right) \hat{Y} + \frac{4}{15} \sqrt{1 + \Lambda \hat{P}_0(\chi^*)} \hat{Y}^{5/2} \sim \hat{\Psi}$$
$$\hat{S} = \mathcal{O}(\hat{L}), \qquad \hat{Y} = \mathcal{O}(\hat{L}^{4/3}) \tag{134}$$

Finally, it should be mentioned that, from a computational point of view, the triple-deck formulation presented here is related to the original numerical treatment of transient marginal separation past the leading edge of an airfoil by Briley and McDonald [44]. They employed an advanced mixing-length-based one-equation closure and adopted a time-dependent iterative scheme that reflects the interaction process, albeit in a nonasymptotic sense. This technique allowed for avoiding the occurrence of the Goldstein singularity in the skin friction in the boundary-layer sweeps and the prediction of closed separation bubbles.

V. Conclusions

An asymptotic theory of turbulent marginal separation has been presented that depends on a single similarity parameter $\chi \ge 0$ containing the essential upstream information. Numerical solutions of the fundamental triple-deck problem have been found for a wide range of χ. Open questions include, among others, the effect of the exponentially decaying eigensolutions as $\hat{X} \to -\infty$ that dominate over the algebraically varying terms for $\Gamma = 1$ in the noninteractive case $\Lambda \to 0$ or, equivalently, $\chi \to \infty$ as predicted by Eq. (124). Then only the strictly attached solutions have been found at present, which are related to the subcritical upstream condition $\gamma < 0$. Its supercritical counterpart $\gamma > 0$, however, causing the boundary-layer solution to terminate in the Goldstein-type singularity, is likely associated with a very large recirculation region if the induced pressure is taken into account in an appropriate manner. That is, the triple-deck problem has to be investigated in order to explore the according substructure that emerges for $\Lambda \to 0$ and predicts separation on a correspondingly larger streamwise length scale. Interestingly, the assumption of an almost inviscid but strongly rotational flow inside the separation region proposed much earlier by Perry and Fairlie [42] is possibly pointed to the inviscid character of the boundary-layer solution slightly upstream of the position of breakdown; see Sec. III.D. This observation may therefore become relevant to the study of large-scale separation.

Furthermore, the effects of the inner wake as well as the Reynolds-number-dependent flow regimes adjacent to the surface have to be studied. However, the inner wake layer, not considered here, is seen to behave only passively, as it is characterized by convective terms linearized about the slip velocity imposed by the outer wake. Because $\alpha \ll 1$ even in the limiting case $Re^{-1} = 0$, the perturbations in the wake regime reflecting viscous effects, which primarily arise from the surface shear stress denoted by τ, are of minor (physical) relevance. On the other hand, most important, matching of the logarithmically varying u components of the velocities in the overlap domain of the viscosity-affected near-wall flow regimes gives rise to a relationship determining the surface friction τ in the limit $Re \to \infty$:

$$\frac{\sqrt{\tau}}{u_s} \sim \frac{\kappa}{\ell_n Re}, \qquad \tau = \frac{1}{Re} \frac{\partial u}{\partial y} \quad \text{at} \quad y = 0 \tag{135}$$

That skin friction law is clearly rendered invalid if the surface slip velocity u_s at the base of the wake tends to zero, which is the case as separation is approached. Therefore, the investigation of a flow on the verge of separation, for which the reverse-flow regime is governed by Eq. (134), is expected to give a first hint how to continue the skin friction law (135) asymptotically correctly into the regions in which the flow separates but immediately recovers. It can be shown [11,12] that both $\sqrt{\tau}$ and u_s become quantities of $\mathcal{O}(1)$, provided that u_s has dropped sufficiently. Then the logarithmic law of the wall is superseded by the half-power behavior of u, well known from a boundary layer on the verge of separation, as the viscous wall layer coincides with the flow regime on top of it (see the outline in Sec. II.B.2), and the relationship (135) ceases to be valid. Because the flow inside the viscous wall layer then plays a fundamental role in order to predict the surface friction, a study of the time-dependent motions in that region is presumably necessary. The basis for such a research is provided by the extensive work of Walker et al. [14], Walker and Herzog [15], and Brinckman and Walker [16] (see also [1]), which, however, applies to a firmly attached turbulent boundary layer.

With respect to those aspects, which are presently under investigation, we add that results obtained by means of direct numerical simulation (DNS) [45] indicate that small changes in the

pressure distribution due to an external flow that triggers the occurrence of a mild separation bubble have a relatively great impact on the skin friction distribution. Here, we stress that this observation is corroborated by the theory presented, as the slip velocity is related to the skin friction through Eq. (135). A qualitative comparison of the theory outlined here with the DNS study of marginal separation by Na and Moin [46], as well as the large-eddy simulation by Cabot [47], for the identical flow configuration is also a topic of current research. Unfortunately, a validation of the theoretical results with experimental data, although highly desirable, appears to be presently impossible on the basis of the existing material.

Acknowledgments

This work was supported by the Austrian Science Fund (FWF) under grant no. P16555-N12. Also, the authors would like to thank the referees for several helpful suggestions and advice that aided to enhance the quality of the paper. The authors also wish to acknowledge David Walker for his outstanding work on turbulent boundary layers (see also [48]).

References

[1] Walker, J. D. A., "Turbulent Boundary Layers 2: Further Developments," *Recent Advances in Boundary Layer Theory*, edited by A. Kluwick, Vol. 390, CISM Courses and Lectures, Springer, New York, 1998, pp. 145–230.

[2] Degani, A. T., Smith, F. T., and Walker, J. D. A., "The Structure of a Three-Dimensional Turbulent Boundary Layer," *Journal of Fluid Mechanics*, Vol. 250, 1993, pp. 43–68.

[3] Degani, A. T., Smith, F. T., and Walker, J. D. A., "The Three-Dimensional Turbulent Boundary Layer Near a Plane of Symmetry," *Journal of Fluid Mechanics*, Vol. 234, 1992, pp. 329–360.

[4] Yajnik, K. S., "Asymptotic Theory of Turbulent Shear Flows," *Journal of Fluid Mechanics*, Vol. 42, No. 2, 1970, pp. 411–427.

[5] Bush, W. B., and Fendell, F. E., "Asymptotic Analysis of Turbulent Channel and Boundary-Layer Flow," *Journal of Fluid Mechanics*, Vol. 56, No. 4, 1972, pp. 657–681.

[6] Fendell, F. E., "Singular Perturbation and Turbulent Shear Flow Near Walls," *Journal of the Astronautical Sciences*, Vol. 20, No. 11, 1972, pp. 129–165.

[7] Mellor, G. L., "The Large Reynolds Number, Asymptotic Theory of Turbulent Boundary Layers," *International Journal of Engineering Science*, Vol. 10, No. 10, 1972, pp. 851–873.

[8] Schlichting, H., and Gersten, K., *Boundary-Layer Theory*, 8th ed., Springer, Berlin, 2000.

[9] Gersten, K., "Turbulent Boundary Layers 1: Fundamentals," *Recent Advances in Boundary Layer Theory*, edited by A. Kluwick, Vol. 390, CISM Courses and Lectures, Springer, Vienna, 1998, pp. 107–144.

[10] Scheichl, B. F., Asymptotic Theory of Marginal Turbulent Separation, Ph.D. Thesis, Vienna Univ.of Technology, Vienna, Austria, June 2001.

[11] Scheichl, B., and Kluwick, A., "On Turbulent Marginal Separation: How the Logarithmic Law of the Wall is Superseded by the Half-Power Law," *Proceedings of the International Conference on Boundary and Interior Layers (BAIL 2006)*, edited by G. Lube and G. Rapin, [CD-ROM], Georg-August Univ. of Göttingen, Göttingen, Germany, 2006; also available at http://www.num.math.uni-goettingen.de/bail/.

[12] Scheichl, B., and Kluwick, A., "Turbulent Marginal Separation: A Novel Triple-Deck Problem for Turbulent Flows," *Progress in Turbulence 2*, edited by J. Peinke, A. Kittel, S. Barth, and M. Oberlack, Proceedings in Physics, Springer, Berlin (to be published).

[13] Nagib, H. M., and Chauhan, K. A., "Scaling of High Reynolds Number Turbulent Boundary Layers Revisited," AIAA Paper 2005-4810, 2005.

[14] Walker, J. D. A., Abbott, D. E., Scharnhorst, R. K., and Weigand, G. G., "Wall-Layer Model for the Velocity Profile in Turbulent Flows," *AIAA Journal*, Vol. 27, No. 2, 1989, pp. 140–149.

[15] Walker, J. D. A., and Herzog, S., "Eruption Mechanisms for Turbulent Flows Near Walls," *Transport Phenomena in Turbulent Flows: Theory, Experiment, and Numerical Simulation*, edited by M. Hirata and N. Kasagi, Hemisphere, New York, 1988, pp. 145–156.

[16] Brinckman, K. W., and Walker, J. D. A., "Instability in a Viscous Flow Driven by Streamwise Vortices," *Journal of Fluid Mechanics*, Vol. 432, 2001, pp. 127–166.

[17] Smith, C. R., and Walker, J. D. A., "Chapter 6: Turbulent Wall-Layer Vortices," *Fluid Vortices*, edited by S. I. Green, Vol. 30, of Fluid Mechanics and its Applications, Kluwer Academic, Dordrecht, 1995, pp. 135–290.

[18] Ruban, A. I., "Singular Solutions of the Boundary Layer Equations Which Can Be Extended Continuously Through the Point of Zero Surface Friction," *Fluid Dynamics*, Vol. 16, No. 6, 1981, pp. 835–843 [English]; also *Izvestiya Akademii Nauk SSSR, Mekhanika Zhidkosti i Gaza*, No. 6, 1981, pp. 42–52 [Russian].

[19] Ruban, A. I., "Asymptotic Theory of Short Separation Regions on the Leading Edge of a Slender Airfoil," *Fluid Dynamics*, Vol. 17, No. 1, 1982, pp. 33–41 [English]; also *Izvestiya Akademii Nauk SSSR, Mekhanika Zhidkosti i Gaza*, No. 1, 1982, pp. 42–51 [Russian].

[20] Stewartson, K., Smith, F. T., and Kaups, K., "Marginal Separation," *Studies in Applied Mathematics*, Vol. 67, No. 1, 1982, pp. 45–61.

[21] Sychev, V. V., Ruban, A. I., Sychev, V. V., and Korolev, G. L., *Asymptotic Theory of Separated Flows*, Cambridge Univ. Press, Cambridge, England, U.K., 1998.

[22] Scheichl, B., and Kluwick, A., "Singular Solutions of the Turbulent Boundary Layer Equations in the Case of Marginal Separation as $Re \to \infty$," *Advances in Turbulence 9: Proceedings of the Ninth European Turbulence Conference*, edited by I. P. Castro, P. E. Hancock, and T. G. Thomas, International Center for Numerical Methods in Engineering (CIMNE), Barcelona, 2002, pp. 829–832.

[23] Neish, A., and Smith, F. T., "On Turbulent Separation in the Flow Past a Bluff Body," *Journal of Fluid Mechanics*, Vol. 241, 1992, pp. 443–467.

[24] Melnik, R. E., "A New Asymptotic Theory of Turbulent Boundary Layers and the Turbulent Goldstein Problem," *Boundary-Layer Separation. Proceedings of the IUTAM Symposium*, edited by F. T. Smith and S. N. Brown, Springer, New York, 1987, pp. 217–234.

[25] Melnik, R. E., "An Asymptotic Theory of Turbulent Separation," *Computers & Fluids*, Vol. 17, No. 1, 1989, pp. 165–184.

[26] Michel, R., Quémard, C., and Durant, R., "Hypothesis on the Mixing Length and Application to the Calculation of the Turbulent Boundary Layers," *Computations of Turbulent Boundary Layers: 1968 AFOSR-IFP-Stanford Conference Proceedings*, edited by S. J. Kline, M. V. Morkovin, G. Sovran, and D. J. Cockrell, Vol. 1, Stanford Univ., Stanford, CA, 1969, pp. 195–207.

[27] Clauser, F. H., "The Turbulent Boundary Layer," *Advances in Applied Mechanics*, edited by H. Dryden and T. von Kármán, Vol. 4, Academic, New York, 1956, pp. 1–51.

[28] Goldstein, S., "On Laminar Boundary Layer Flow Near a Position of Separation," *Quarterly Journal of Mechanics and Applied Mathematics*, Vol. 1, No. 1, 1948, pp. 43–69.

[29] Stewartson, K., "Is the Singularity at Separation Removable?," *Journal of Fluid Mechanics*, Vol. 44, No. 2, 1970, pp. 347–364.

[30] Schneider, W., "Boundary-Layer Theory of Free Turbulent Shear Flows," *Zeitschrift für Flugwissenschaften und Weltraumforschung (Journal of Flight Sciences and Space Research)*, Vol. 15, No. 3, 1991, pp. 143–158.

[31] Klebanoff, P. B., "Characteristics of Turbulence in a Boundary Layer with Zero Pressure Gradient," NACA TR 1247, 1955; also NACA TN 3178, 1954.

[32] Skåre, P. E., and Krogstadt, Å. -P., "A Turbulent Equilibrium Boundary Layer Near Separation," *Journal of Fluid Mechanics*, Vol. 272, 1994, pp. 319–348.

[33] Rothmayer, A. P., and Smith, F. T., "High Reynolds Number Asymptotic Theories," *The Handbook of Fluid Dynamics*, Part 3, edited by R. W. Johnson, CRC Press, Boca Raton, FL, and Springer, Heidelberg, Germany, 1998, pp. 23.1–25.26.

[34] Messiter, A. F., "Boundary-Layer Flow Near the Trailing Edge of a Flat Plate," *SIAM Journal on Applied Mathematics*, Vol. 18, No. 1, 1970, pp. 241–257.

[35] Stewartson, K., "On the Flow Near the Trailing Edge of a Flat Plate II," *Mathematika*, Vol. 16, No. 1, 1969, pp. 106–121.

[36] Abramowitz, M., and Stegun, I. A., *Handbook of Mathematical Functions*, 9th ed., Dover, New York, 1972.

[37] Lipatov, I. I., "On the Theory of Separation of a Laminar Boundary Layer in a Supersonic Flow," *Fluid Dynamics*, Vol. 19, No. 4, 1984, pp. 555–560 [English]; also *Izvestiya Akademii Nauk SSSR, Mekhanika Zhidkosti i Gaza*, No. 4, 1984, pp. 51–56 [Russian].

[38] Smith, F. T., and Merkin, J. H., "Triple-Deck Solutions for Subsonic Flows Past Humps, Steps, Concave or Convex Corners and Wedged Trailing Edges," *Computers & Fluids*, Vol. 10, No. 1, 1982, pp. 7–25.

[39] Cassel, K. W., Ruban, A. I., and Walker, J. D. A., "An Instability in Supersonic Boundary-Layer Flow Over a Compression Ramp," *Journal of Fluid Mechanics*, Vol. 300, 1995, pp. 265–285.

[40] Gajjar, J. S. B., and Türkyılmazoğlu, M., "On the Absolute Instability of the Triple-Deck Flow Over Humps and Near Wedged Trailing Edges," *Philosophical Transactions of the Royal Society of London*, Series A: Mathematical, Physical and Engineering Sciences, Vol. 358, No. 1777, 2000, pp. 3113–3128.

[41] Powell, M. J. D., "A Hybrid Method for Nonlinear Algebraic Equations," *Numerical Methods for Nonlinear Algebraic Equations*, edited by P. Rabinowitz, Gordon and Breach, London, 1970, Chap. 6, pp. 87–114.
[42] Perry, A. E., and Fairlie, B. D., "A Study of Turbulent Boundary-Layer Separation," *Journal of Fluid Mechanics*, Vol. 69, No. 4, 1975, pp. 657–672.
[43] Cutler, A. D., and Johnston, J. P., "Adverse Pressure Gradient and Separating Turbulent Boundary Flows: The Effect of Disequilibrium in Initial Conditions," Stanford Univ. Thermosciences Div., Mechanical Engineering Dept., Rept. MD-46, Stanford, CA, 1984.
[44] Briley, W. R., and McDonald, H., "Numerical Prediction of Incompressible Separation Bubbles," *Journal of Fluid Mechanics*, Vol. 69, No. 4, 1975, pp. 631–656.
[45] Skote, M., and Henningson, D. S., "Direct Numerical Simulation of a Separated Turbulent Boundary Layer," *Journal of Fluid Mechanics*, Vol. 471, 2002, pp. 107–136.
[46] Na, Y., and Moin, P., "Direct Numerical Simulation of a Separated Turbulent Boundary Layer," *Journal of Fluid Mechanics*, Vol. 374, 1998, pp. 379–405.
[47] Cabot, W., "Large-Eddy Simulation of a Separated Boundary Layer," *Annual Research Briefs - 1998 (Center for Turbulence Research)*, NASA Ames Research Center and Stanford Univ., Stanford, CA, 1998, pp. 279–287.
[48] Scheichl, B., and Kluwick, A., "Turbulent Marginal Separation and the Turbulent Goldstein Problem," AIAA Paper 2005-4936, 2005.

A. Tumin
Associate Editor